UNIVERSITY OF ILLINOIS
URBANA

AERONOMY REPORT NO. 64

STUDIES OF THE DIFFERENTIAL ABSORPTION ROCKET EXPERIMENT

by
J. C. Ginther
L. G. Smith

January 15, 1975

Library of Congress ISSN 0568-0581

Supported by
National Aeronautics and Space Administration
NGR 14-005-181

Aeronomy Laboratory
Department of Electrical Engineering
University of Illinois
Urbana, Illinois

CITATION POLICY

The material contained in this report is preliminary information circulated rapidly in the interest of prompt interchange of scientific information and may be later revised on publication in accepted aeronomic journals. It would therefore be appreciated if persons wishing to cite work contained herein would first contact the authors to ascertain if the relevant material is part of a paper published or in process.

UILU-ENG 75 2501

A E R O N O M Y R E P O R T

N O. 64

STUDIES OF THE DIFFERENTIAL ABSORPTION ROCKET EXPERIMENT

By

J. C. Ginther
L. G. Smith

January 15, 1975

Supported By
National Aeronautics
and Space Administration
Grant NGR 14-005-181

Aeronomy Laboratory
Department of Electrical Engineering
University of Illinois
Urbana, Illinois

ABSTRACT

Investigations of the ionosphere, in the rocket program of the Aeronomy Laboratory, include a propagation experiment, the data from which may be analyzed in several modes. This report considers in detail the differential absorption experiment. The sources of error and limitations of sensitivity are discussed. Methods of enhancing the performance of the experiment are described. Some changes have been made in the system and the improvement demonstrated. Suggestions are made for further development of the experiment.

TABLE OF CONTENTS

LIST OF TABLES

LIST OF FIGURES

1. INTRODUCTION

The propagation experiment has been used on all rocket flights conducted by NASA for the University of Illinois' Aeronomy Laboratory. The experiment was designed by the Coordinated Science Laboratory for use in the IQSY years of 1964 and 1965. The experiment measures two phenomena, differential absorption and Faraday rotation. Faraday rotation is the phenomenon of the changing phase characteristics between two propagating modes, while differential absorption is characterized by a difference in attenuation rates. These two phenomena can be used together to determine electron concentrations and electron collision frequencies, or independently, by use of suitable approximation, for calculation of electron densities. The electron densities used to calibrate probe experiments, carried by the rockets, are capable of measuring fine structure in the electron concentration, but not absolute magnitudes.

This report is concerned with operation of the differential absorption experiment without use of the accompanying Faraday rotation data. The objectives are to determine criteria for determining valid data and improvement of the accuracy of measurements. It is desired to be able to measure electron concentrations as low as 10 cm^{-3}. To accomplish this the errors in the absorption rates measured on daytime flights must be reduced to about .01 dB/sec. For nighttime flights the objective is to reduce the errors from values over 1 dB/sec often seen, to values of about .1 dB/sec.

Chapter 2 gives a summary of the theory of the propagation experiment as it applies to differential absorption. Chapter 3 describes

improvements made in the operating and data-reduction systems. Chapter 4 covers errors in the experiment resulting from unwanted signals which are not included in the theory of the experiment's design. Chapter 5 discusses the range of valid data and how this should be defined in future work. Finally, Chapter 6 contains suggestions for system improvements which can be made without major redesign of the experiment.

2. THEORY AND IMPLEMENTATION OF THE PROPAGATION EXPERIMENT

To gain an understanding of how the propagation experiment is designed to operate, the theory developed by *Appleton* [1932] and *Hartree* [1931] provides an excellent working base. This theory has been improved upon by *Sen and Wyller* [1960] but the Appleton-Hartree equations provide the necessary tools to understand the experiment and are the basis upon which the experiment was designed.

The following sections will present an outline of the Appleton-Hartree theory and how this is changed by Sen and Wyller. Then a description of how the experiment is designed and an outline of the data reduction process will be presented.

2.1 *The Theory of Appleton-Hartree Under Quasi-Longitudinal Propagating Conditions*

In a region of free electrons, such as the earth's ionosphere, where there is a magnetic field present the medium becomes bi-refringent. This means that a traveling wave entering this medium will be split into two elliptically polarized modes, each mode subject to a different index of refraction. The theory of Appleton-Hartree determines the modes of propagation and the indexes of refraction of these modes in the earth's ionosphere under the following assumptions: electron collisions with neutrals are independent of electron energies, the medium of propagation is electrically neutral with a uniform charge distribution, the magnetic field is uniform throughout the medium, and the ions, because their masses are much greater than that of an electron, are stationary. The theory follows:

Assume a vertically propagating wave which has the form

$$\underline{E} = E_o \exp[j(\omega t - kz)] \tag{2.1}$$

k is the propagation constant, ω is the operation frequency, and E_o a reference field

$$E_o = E_x \hat{x} + E_y \hat{y} . \tag{2.2}$$

The polarization of this wave is defined as

$$R = \frac{E_x}{E_y} . \tag{2.3}$$

If the fields are in the form of equation (2.2) they will have refraction indices given by

$$n^2 = 1 + \frac{P_x}{E_o E_x} = 1 + \frac{P_y}{E_o E_y} = \frac{k}{\omega\sqrt{E_o \mu_o}} . \tag{2.4}$$

In the above, P_x and P_y are the polarization fields in the x and y directions. The motion of the free electrons in the ionosphere will be governed by the equation of motion:

$$m\ddot{\underline{r}} + m\nu\dot{\underline{r}} = - e(\dot{r} \times \underline{B}) - e\underline{E} . \tag{2.5}$$

ν is the electron-neutral collision frequency, and $\underline{B}$ the magnetic flux. The polarization can be found from the electron displacements as

$$\underline{P} = - N e \underline{r} \tag{2.6}$$

where N is the electron density.

Before continuing the development of the theory, the following table of standard symbols is presented.

$$Z = \frac{\nu}{\omega}$$

$$X = \frac{\omega N^2}{\omega^2}$$

$$\underline{Y} = \frac{\underline{\omega} H}{\omega}$$

ω_N is the plasma frequency and is defined as

$$\omega_N = \frac{Ne^2}{E_o} .$$

ω_H is the gyrofrequency defined as

$$\underline{\omega}_H = \frac{e\underline{B}}{m}$$

which is divided into two components, one along the direction of propagation and one transverse to the propagating wave.

With the above set of symbols, equations (2.5) and (2.6) can be combined to form

$$E_o \underline{E} = M^{-1} \underline{P} \tag{2.7}$$

where

$$M^{-1} = -X^{-1} \begin{pmatrix} 1 - jZ & jY_L & -jY_T \\ -jY_L & 1 - jZ & 0 \\ jY_T & 0 & 1 - jZ \end{pmatrix}$$

When this result is combined with Maxwell's equations, the characteristic equation for the polarization becomes

$$R^2 + j \frac{Y_T^2/Y_L}{1-X-jZ} R + 1 = 0 \tag{2.8}$$

which when solved for the polarization yields

$$R = -j \left[\frac{Y_T^2/2Y_L}{-X-jZ} \mp \sqrt{1 + \frac{Y_T^4/4Y_L^2}{1+X-jZ}} \right] \tag{2.9}$$

and the solution for the refractive index is

$$n^2 = 1 - \frac{X}{1 - jZ - jY_L R} \tag{2.10}$$

which is known as the Appleton-Hartree formula.

For rocket flights from Wallops Island, with which this study has been primarily concerned, the equations can be simplified since the direction of propagation is approximately along a magnetic field line so that

$$\left| \frac{Y_T^2}{2Y_L} \right| << \left| 1 - X - jZ \right|$$

is valid.

When this approximation is used in equations (2.9) and (2.10), the results are

$$R = \pm j \tag{2.11}$$

$$n^2 = 1 - \frac{X}{1-jZ \pm Y_L} \tag{2.12}$$

The solution for R indicates two circular modes will be propagated. The $+j$ is known as the extraordinary mode and the $-j$ as the ordinary. In the refractive index relation, the plus sign on Y_L is associated with the ordinary mode and the minus with the extraordinary mode.

A further approximation in the equations may be made on the basis that the plasma frequency in the D and E regions where the experiment is intended to be used, is much smaller than the frequency of the propagating wave used in the experiments, thus

$$X << 1 \tag{2.13}$$

Using (2.13) in (2.12) yields

$$n = 1 - \frac{\frac{1}{2}X}{1-jZ \pm Y_L} \tag{2.14}$$

The index of refraction is divided into its real and imaginary parts

$$n = m + j\,\chi \tag{2.15}$$

$$n = \left(1 - \frac{\frac{1}{2}X\,(1 \pm Y_L)}{(1 \pm Y_L)^2 + Z^2}\right) - j\left(\frac{\frac{1}{2}XZ}{(1 \pm Y_L)^2 + Z^2}\right)$$

and the equation for the propagating wave may be written as

$$\underline{E} = E_o \exp(-\chi k_o Z) \exp[j(\omega t - \mu k_o Z] \tag{2.16}$$

This is the equation of a wave which decays in amplitude as it propagates. It is this phenomena described by the coefficient of absorption

$$K = k_o\,\chi \tag{2.17}$$

with which this study is concerned.

2.2 *The Sen-Wyller Theory*

An improvement on the Appleton-Hartree theory was developed by *Sen and Wyller* [1960] to correct the assumption that the collision frequency is independent of electron energy. The collision frequency is assumed to have the form

$$\nu = \nu_m\, f(v) \tag{2.18}$$

$f(v)$ is a function of the electron velocity which is assumed to be Maxwellian. The theory is quite complicated and will not be reproduced here.

The result of the theory is to give an index of refraction

$$n = \frac{A + B \sin^2\psi \pm B^2 \sin^4\psi - C^2 \cos^2\psi}{D + E \sin^2\psi} . \qquad (2.19)$$

ψ is the angle between the wave normal and $\underline{B}$, with the other variables defined as follows:

$$A = 2\,\varepsilon_I(\varepsilon_I + \varepsilon_{III})$$

$$B = \varepsilon_{III}(\varepsilon_I + \varepsilon_{III})$$

$$C = 2\,\varepsilon_I\varepsilon_{II}$$

$$D = 2\,\varepsilon_I$$

$$E = 2\,\varepsilon_{III}$$

ε_I, ε_{II}, and ε_{III} are the dielectric tensor elements defined as

$$\varepsilon_I = (1-a) - j\,b$$

$$\varepsilon_{II} = (f-d)/2 + i(c-e)/2$$

$$\varepsilon_{III} = [a-(c+e)/2] + j\,[b - (f+d)/2],$$

in which a, b, c, d, e, and f are functions of the $\mathcal{G}$ script integrals

$$\zeta_p(x) = \frac{1}{p!} \int_0^\infty \frac{\varepsilon^p}{(\varepsilon^2 + X^2)} e^{-\varepsilon} \, d\varepsilon \tag{2.20}$$

$$a = \frac{\omega_N^2}{\nu_m} \zeta_{1.5} \left(\frac{\omega}{\nu_m} \right)$$

$$b = \frac{5\,\omega_N^2}{2\omega\nu_m} \zeta_{2.5} \left(\frac{\omega}{\nu_m} \right)$$

$$c = \frac{N^2(\omega-\omega_H)}{\omega\nu_m^2} \zeta_{1.5} \left(\frac{\omega-\omega_H}{\nu_m} \right)$$

$$d = \frac{5\omega_N^2}{2\omega\nu_m} \zeta_{2.5} \left(\frac{\omega-\omega_H}{\nu_m} \right)$$

$$e = \frac{\omega_N^2 (\omega+\omega_H)}{\omega\nu_m^2} \zeta_{1.5} \left(\frac{\omega+\omega_H}{\nu_m} \right)$$

$$f = \frac{5\omega_N^2}{2\omega\nu_m} \zeta_{2.5} \left(\frac{\omega+\omega_H}{\nu_m} \right)$$

Figure 2.1 shows how the Sen-Wyller and Appleton-Hartree theories differ, especially at high collision frequencies found at the lower altitudes. It is clear from this that the full Sen-Wyller theory will be necessary for analysis below 85 km.

2.3 *Operation of the Experiment*

In order to measure the absorption properties of the atmosphere, the two modes are transmitted from the ground to a rocket as it passes through

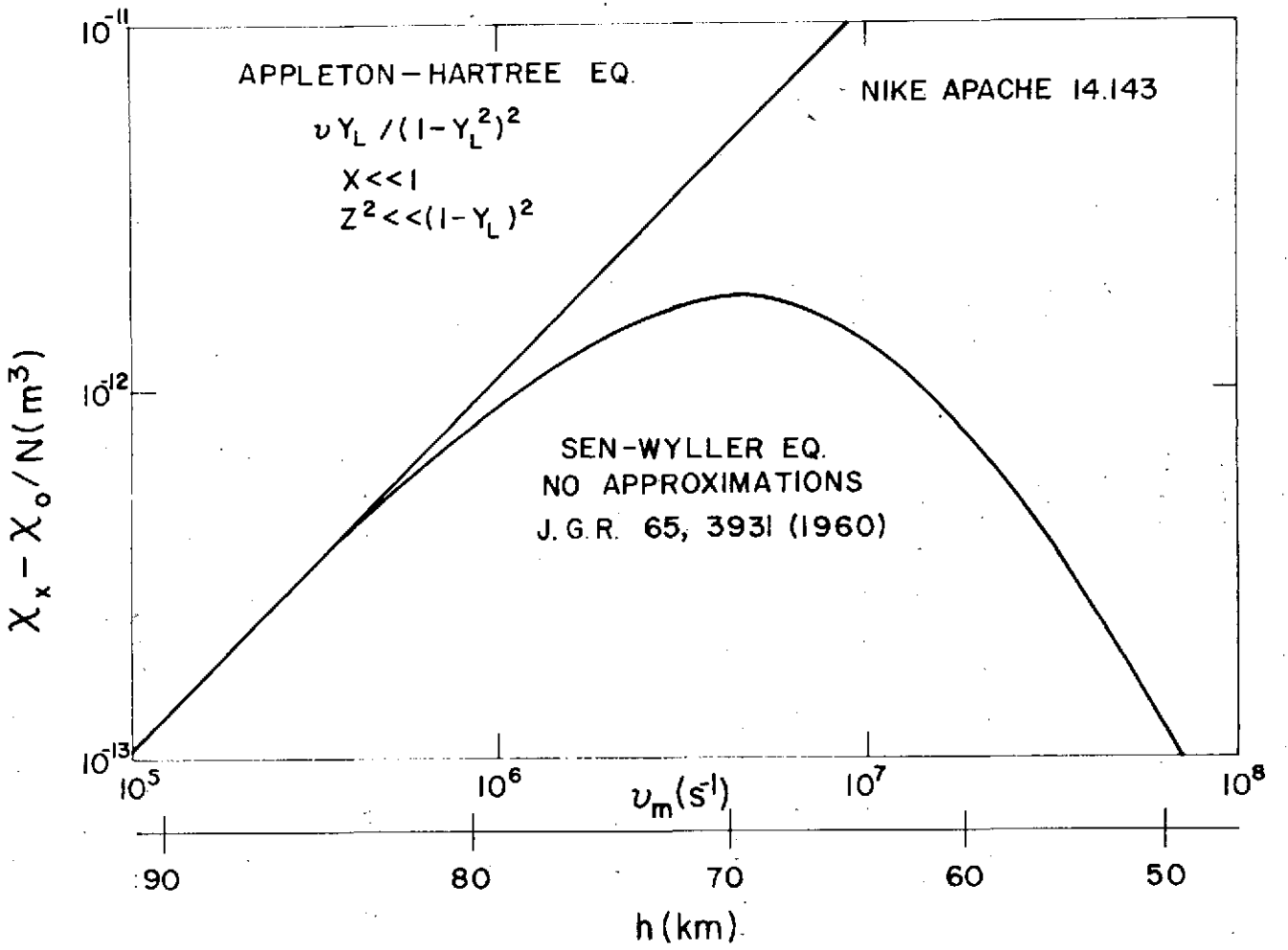

Figure 2.1 Appleton-Hartree versus Sen-Wyller differential absorption index per unit electron concentration as a function of electron collision frequency. The approximate Appleton-Hartree curve is normalized to agree with Sen-Wyller curve for vanishing collision frequency [*Mechtly et al.*, 1967].

the ionosphere. By measuring the differences in the rate of absorption of the two modes (differential absorption) and combining the results with the Faraday rotation experiment, or by using a collision frequency model, the electron concentration of the ionosphere can be measured.

A block diagram of the original system is shown in Figure 2.2. The signal generated by the configuration consists of an ordinary wave at frequency $f_o - \delta$, where δ is 250 Hz, and an extraordinary wave at $f_o + \delta$. The resultant wave can be visualized as an electric vector of frequency f_o spinning in the ordinary direction with a frequency $f_o - \delta$. The magnitude of the vector is governed by an ellipse spinning at frequency δ in the ordinary direction as shown in Figure 2.3. The above assumes the ordinary magnitude is larger than the extraordinary and that δ is positive.

Analytically, the result can be shown by taking the ordinary wave to be

$$\hat{i}\, Q \sin[(\omega-\delta)t - k_o Z] - \hat{j}\, Q \cos[(\omega-\delta)t - k_o Z]$$

The extraordinary wave is then taken as

$$\hat{i}\, R \sin[(\omega+\delta)t - k_x Z] + \hat{j}\, R \cos[(\omega+\delta)t - k_x Z]$$

k_o and k_x are the propagation constants for the o(ordinary) wave and the x(extraordinary) wave.

The unit vector for the rocket antenna spinning at ω_r may be written as

$$\underline{a} = -\hat{i} \sin\omega_r t + \hat{j} \cos\omega_r t \qquad (2.21)$$

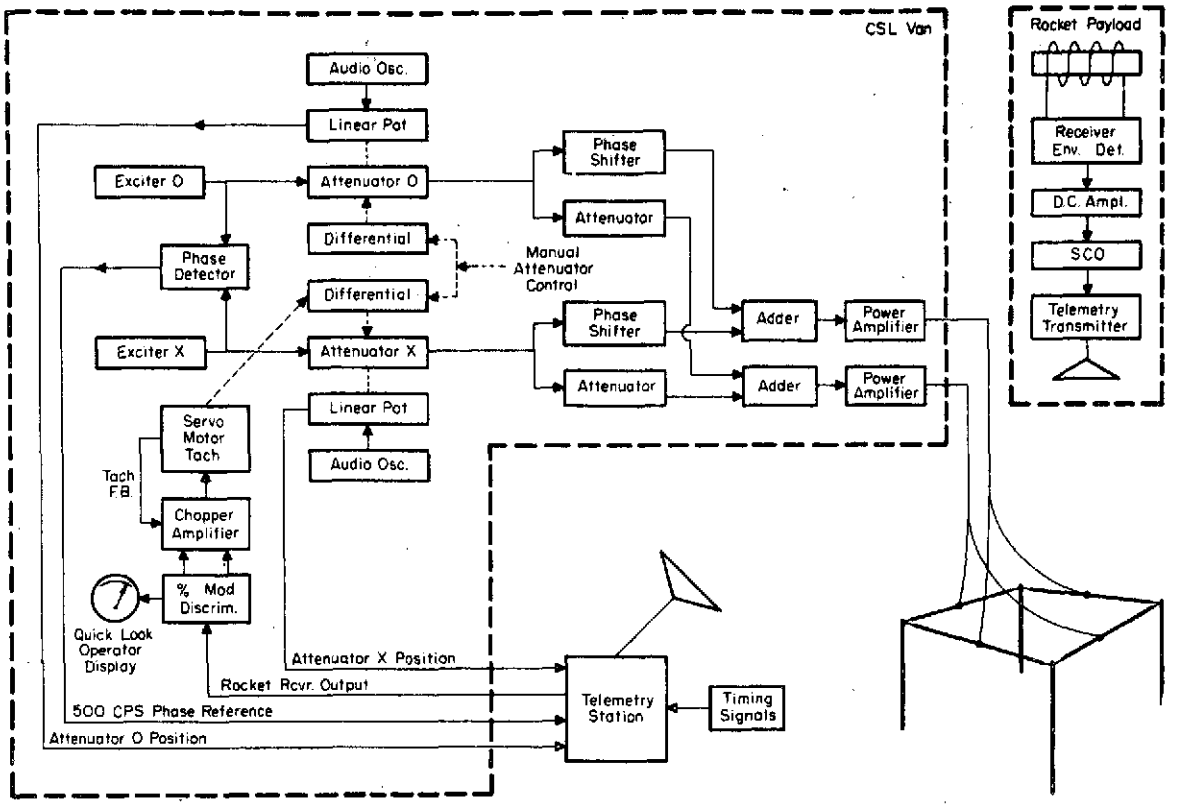

Figure 2.2 Original system block diagram [*Knoebel et al.*, 1965].

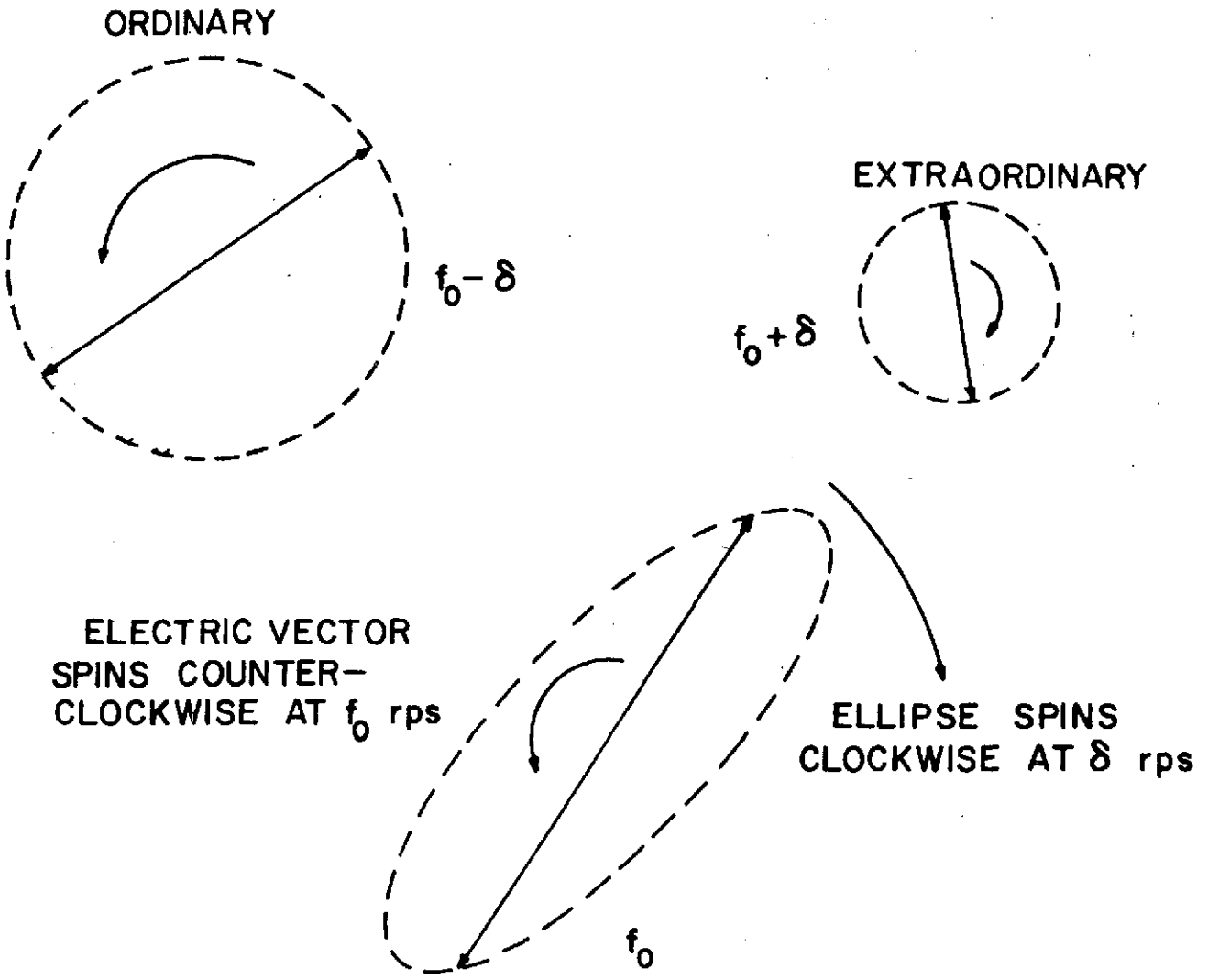

Figure 2.3 Generation of polarization ellipse (adapted from *Salah and Bowhill* [1966]).

Now by substituting in $Z = v_r t$, v_r being the rocket velocity, the total signal received by the antenna is proportional to

$$\underline{E} \cdot \underline{a} = \tag{2.22}$$

$$-[Q \sin(\omega-\delta-k_o v_r)t + R \sin(\omega+\delta-k_x v_r)t] \sin\omega_r t + [-Q \cos(\omega-\delta-k_o v_r)t$$

$$+ R \cos(\omega+\delta-k_x v_r)t] \cos\omega_r t + -Q \cos(\omega-\delta-k_o v_r-\omega_r)t + R \cos(\omega+\delta-k_x v_r+\omega_r)t$$

Making the substitutions

$$A = (-\delta - k_o v_r - \omega_r)t$$

$$B = (\delta - k_x v_r + \omega_r)t$$

The output can be written as

$$-Q[\cos A \cos\omega t - \sin A \sin\omega t] + R[\cos B \cos\omega t - \sin B \sin\omega t] \tag{2.23}$$

$$= [-Q \cos A + R \cos B] \cos\omega t + [Q \sin A - R \sin B] \sin\omega t$$

By employing $e^{j\omega t} = \cos\omega t + j \sin\omega t$ the above can be written

$$Re[(-Q \cos A + R \cos B)\, e^{j\omega t}] + Im[(Q \sin A - R \sin B)\, e^{j\omega t}] \tag{2.24}$$

$$= Re[(-Q \cos A + R \cos B - jQ \sin A + jR \sin B)\, e^{j\omega t}]$$

The receiver detects the amplitude of the coefficient of $e^{j\omega t}$ which is

$$[Q^2 + R^2 - 2QR(A - B)]^{1/2}$$

which may be approximated by

$$(Q^2 + R^2)^{1/2} \left[1 - \frac{QR}{Q^2+R^2} \cos(2\delta - (k_o - k_x)v_r + \omega_r)t\right]$$

The resulting output can be seen to consist of a dc component and one at $2\delta - (k_o - k_x)v_r + 2\omega_r$ rad/sec.

The receiver output is telemetered to the ground and transferred to the transmitting van over data lines. At the van, the dc and $2\delta + 2\omega_r$ components ($(-k_o + k_x)v_r$ is assumed small) are compared in the percent modulation detector. The modulation is kept at a constant percent, and thus the axial ratio of the ellipse at the rocket is kept constant, by adjustment of the transmitted powers of the extraordinary and ordinary waves. This is accomplished by a servo motor which is controlled by the output of the modulation detector. The servo moves a coil within a waveguide beyond cutoff. This acts as an attenuator which is logarithmic in voltage and thus linear in dB. The position of the potentiometer, which is used to measure the attenuation factor, is then recorded to give a record of the rate at which power was added to the *X* wave. The two methods of getting the potentiometer information to the recorders, AM and FM, are discussed in Chapter 3. Figures 2.4 and 2.5 show examples of the outputs on a chart record.

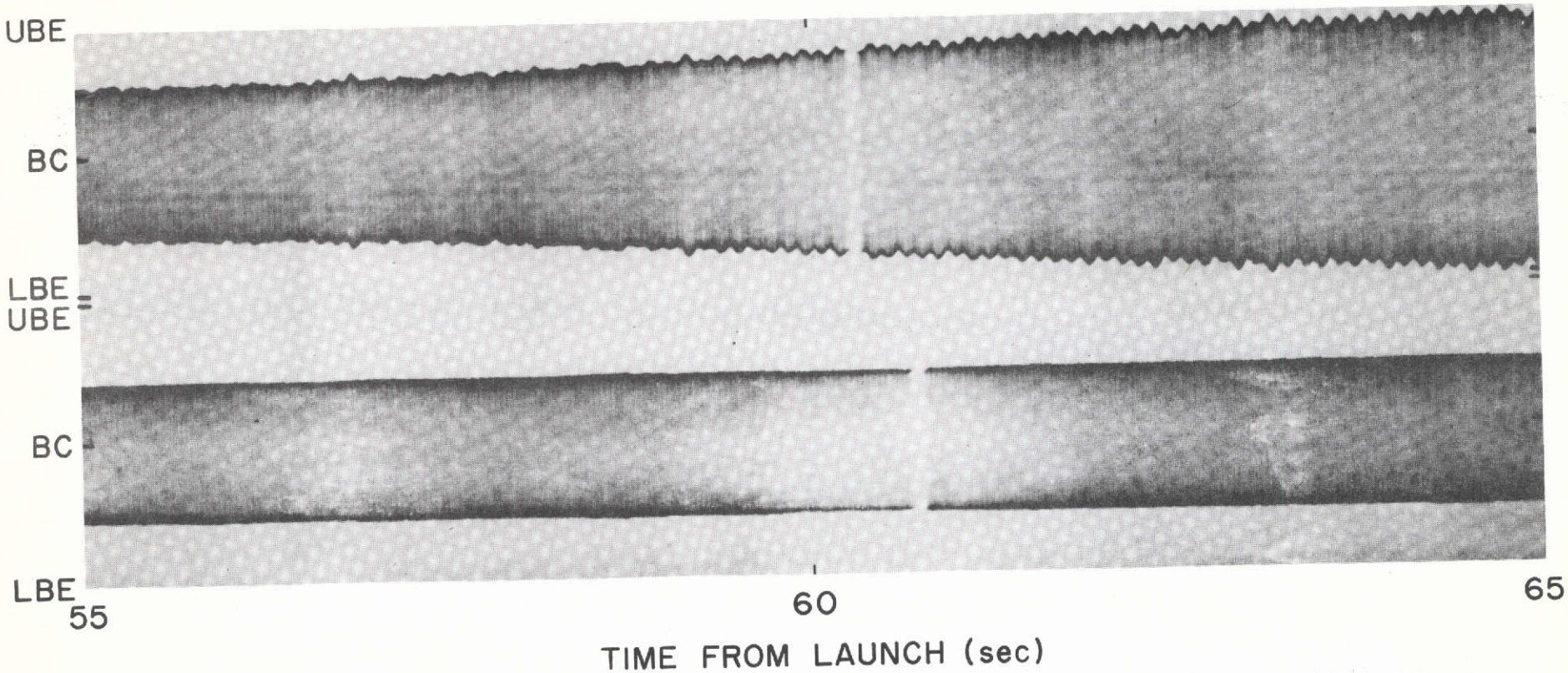

Figure 2.4 Section of chart record for Nike Apache 14.513 showing differential absorption signals in relation to lower band edge (LBE), band center (BC) and upper band edge (UBE). This illustrates the AM system.

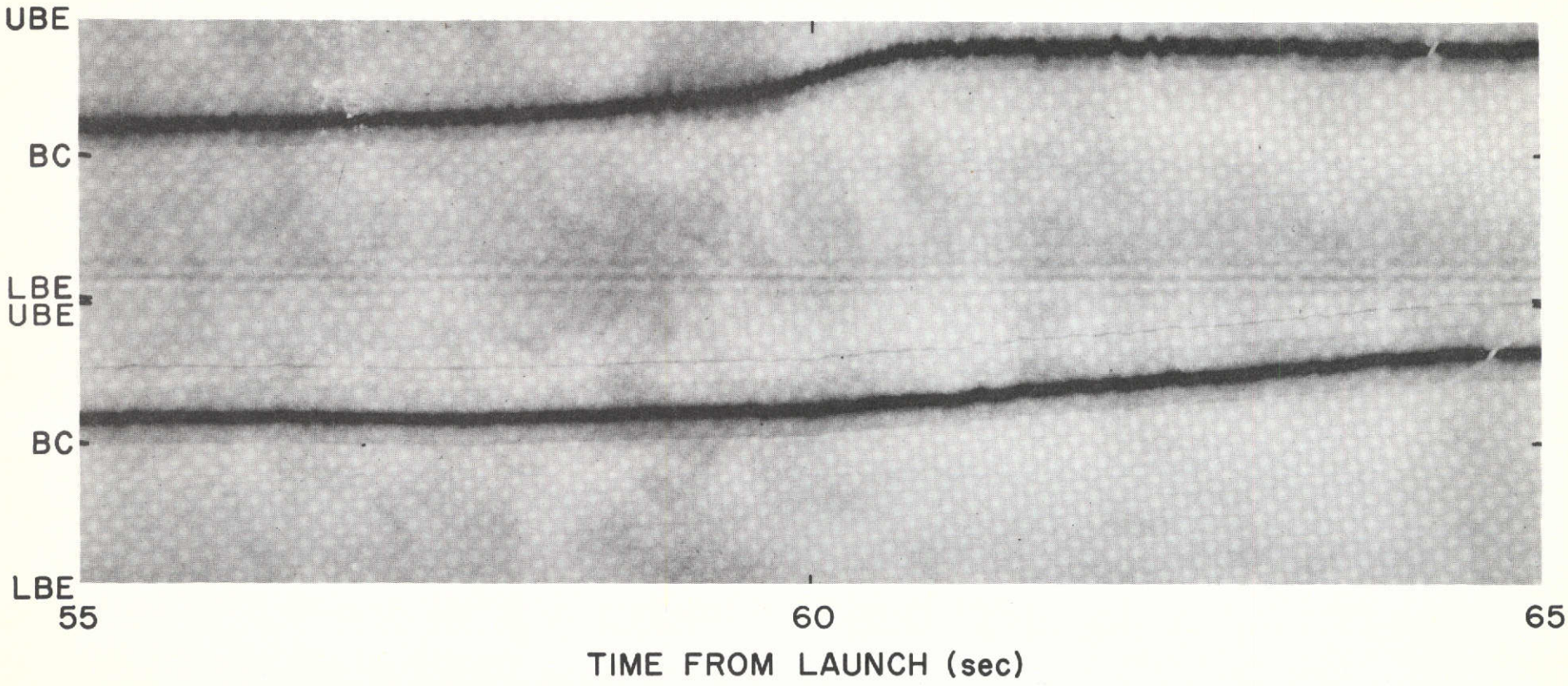

Figure 2.5 Section of chart record for Nike Apache 14.511 showing differential absorption signals in relation to lower band edge (LBE), band center (BC) and upper band edge (UBE). This illustrates the FM system.

2.4 *Procedures for Recovering Rates of Differential Absorption*

Recovery of rates of absorption data to the time of this writing, has made use of CDC 1700 and IBM 360 computers. The 1700 is being replaced and its portion of the reduction process will also be circumvented by use of digital tapes prepared by NASA, since the 1700 is not used in actual reduction but as a means of getting data from the analog to the digital form.

The first step in the process of rate recovery is to convert the information contained in the analog tapes to a digital format suitable for analysis on the IBM 360 computer. Figure 2.6 is a block diagram of the system used for this process. The signals representing the time of data, position of the extraordinary power potentiometer and a 100 kHz reference signal are desired from the tape. The 100 kHz signal is used to measure any tape speed variations and feeds a corrective signal to the discriminator processing the extraordinary power signal. Errors in amplitude in the time signal do not cause errors in the time interpreted, so there is no need to correct this signal. After detection, the time signal is still in a modulated form and is processed by the time code demodulator which sends the proper signal to the digitizing unit.

The output of the extraordinary discriminator is either sent directly to the digitizer in the cases where the FM system of potentiometer position recording is used or to a rectifier when the AM system is employed. The rectifier detects the amplitude and this is then transferred to the digitizer. The outputs of the digitizer are placed onto digital tape by the CDC 1700 computer. This tape is used with the IBM 360 for all further processing.

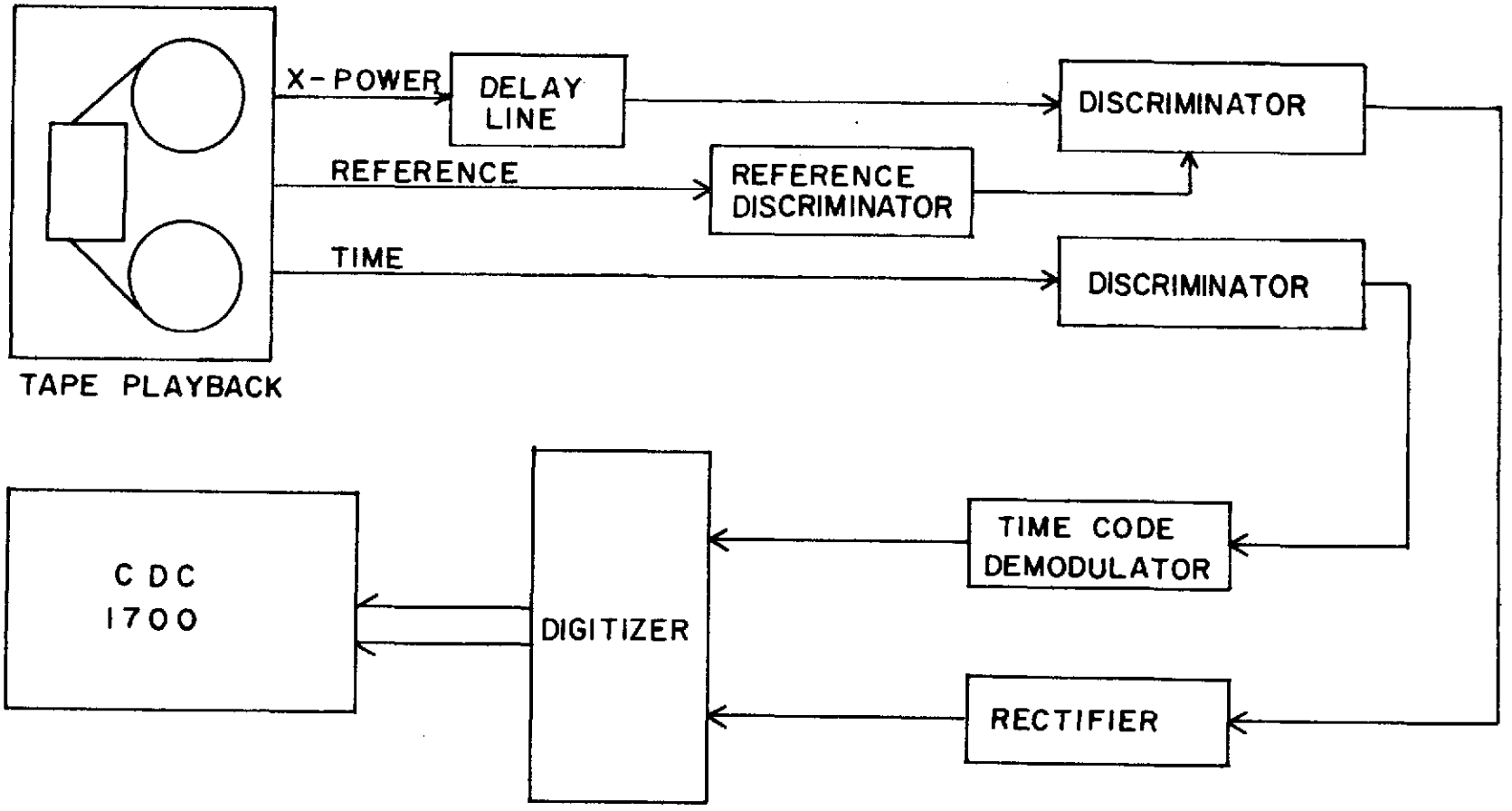

Figure 2.6 Block diagram of digitizing process.

On the 360, DACAL is run first. It processes the data from the preflight calibrations to determine which signal levels correspond to given attenuator settings.

The final step of recovering the rates of absorption is accomplished through program DAPROC. This program analyzes the data on the tape and gives an output of rates of differential absorption in dB/sec. The program may also be directed to punch cards with the differential absorption rates and complete trajectory data for the rocket. This is needed as input for the program which analyzes the data to determine electron concentrations.

2.4.1 *Computer determination of electron concentration from differential absorption rates. Mechtly et al.* [1967] discuss the evaluation of electron concentrations when Faraday rotation data are available. We will deal here with the evaluation of these data in the absence of Faraday rotation.

If the rocket trajectory and the characteristic of the magnetic field are known the only unknown in the equations for determining how each mode is absorbed are collision frequency and electron concentration. To solve for the electron concentration, a model for the collision frequency must be used. It is assumed that the collision frequency is proportional to pressure.

$$\nu_m = C \times 10^5 \, p(z) \tag{2.25}$$

The problem of determining C is discussed by *Mechtly* [1974].

With the value of C chosen, and given pressures taken from 1972, the necessary information to solve for the electron density is at hand. The program assumes an initial electron density and then applies the exact form of the Sen-Wyller equations to determine a differential absorption rate. This is compared with the measured rate and the assumed electron density modified. This process is repeated six times after which it usually has converged to within better than one percent.

3. IMPROVEMENTS MADE IN DATA ACQUISITION AND REDUCTION SYSTEMS

As stated in the Introduction, one of the objectives of this project was to find ways to improve the data, specifically at low altitudes. In an effort to improve the operation of the data acquisition and reduction systems, several of the components making up the differential absorption experiment have been improved. This chapter will examine why the AM data link was replaced by the new FM system and the resulting improvement. Then the operation of tape speed compensation will be reviewed and its effects on the data discussed. Finally the possible use of filtering to recover data from the AM system will be reviewed.

3.1 *FM Data System*

3.1.1 *Theoretical superiority of frequency over amplitude modulation as a data link.*

Part of the original equipment in the University of Illinois van consisted of an amplitude modulated link to transmit the information about the attenuator position to the recording station. This system, shown in Figure 3.1, simply generated a signal with an amplitude proportional to the attenuator position. Due to age, the performance of the four oscillators was degraded and replacements became necessary. With the necessity of replacement, the possible use of a frequency modulated system was examined to see if improvement could be made.

For transmission systems, the figure of merit may be used as a basis of comparison. The figure of merit is defined as the signal-to-noise ratio out of a receiver, divided by the signal-to-noise ratio of the incoming signal,

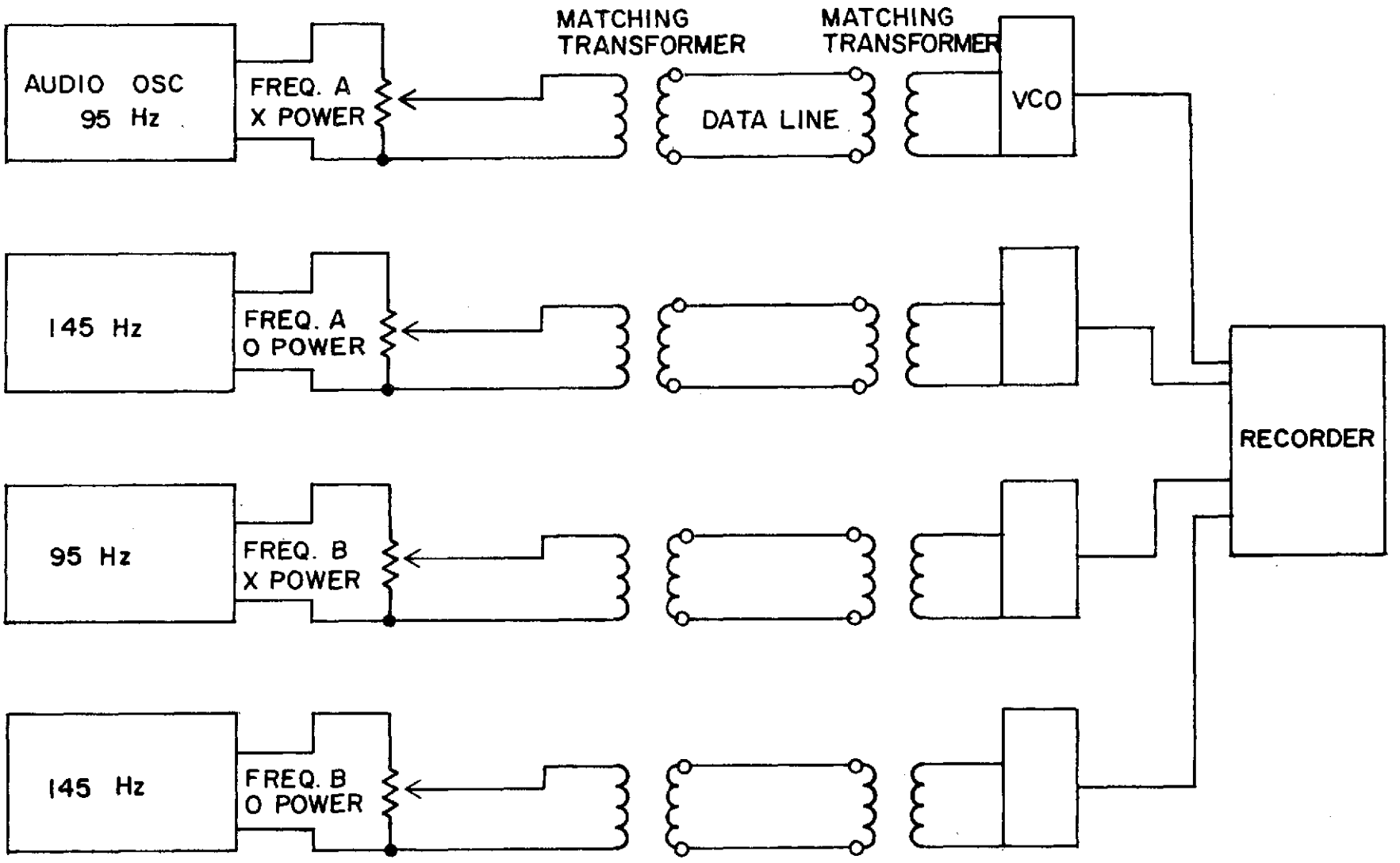

Figure 3.1 Block diagram of amplitude modulated data link.

$$\gamma = \frac{S_o/N_o}{S_i/N_M} \tag{3.1}$$

with N_M being the noise power within the receiver bandwidth.

For an AM system with a signal $Am(t)\cos 2\pi f_c t$, γ was found by *Taub and Schilling* [1971] to be

$$\gamma = \frac{\overline{m^2(t)}}{1 + \overline{m^2(t)}} \tag{3.2}$$

where $\overline{m^2(t)}$ is the mean square value of the modulation coefficient.

For the period of the flight when the differential absorption is just beginning, the signal can be approximated by a sinusoid of amplitude C leading to a figure of merit

$$\gamma_{AM} = \frac{C^2}{2 + C^2} \tag{3.3}$$

For an FM system under the influence of a sinusoid, Taub and Schilling show that

$$\gamma_{FM} = \frac{3}{2} B^2 \tag{3.4}$$

B is the modulation index for the FM signal, f/f_M, f_m being the maximum frequency deviation. Since the same potentiometers would be used in the FM system it will have the same modulation index as the AM system, $B = C$. With this

$$\gamma_{FM} = \frac{3}{2} C^2 \tag{3.5}$$

To compare the two systems the ratio of their figures of merit will be used

$$\frac{\gamma_{FM}}{\gamma_{AM}} = \frac{\frac{3}{2} C^2}{\frac{C^2}{2 + C^2}} = \frac{3}{2} (2 + C^2) = 3 + \frac{3}{2} C^2 \quad . \tag{3.6}$$

This indicated that the implementation of an FM system will improve the noise rejection of the data transfer process by more than three. Because of this result, an FM link was installed.

3.1.2 *Design of frequency modulated data link.* Figure 3.2 shows how the FM system was implemented. To minimize alterations to the system, as few changes as possible were introduced. In place of the four audio oscillators of the AM system, a single precision dc supply was installed. The voltages present at the variable contacts of the potentiometers are then used as the inputs to voltage controlled oscillators.

To choose the VCO frequencies, tests were run on the data lines at Wallops Island, Virginia, to determine their frequency response characteristics. Figure 3.3 gives the frequency responses of four data lines and the locations of IRIG proportional bandwidth channels 1 through 10. It is desirable to use the highest useful frequencies since the data rate increases with the higher channels. Under these restrictions, channels 4 through 7 were selected.

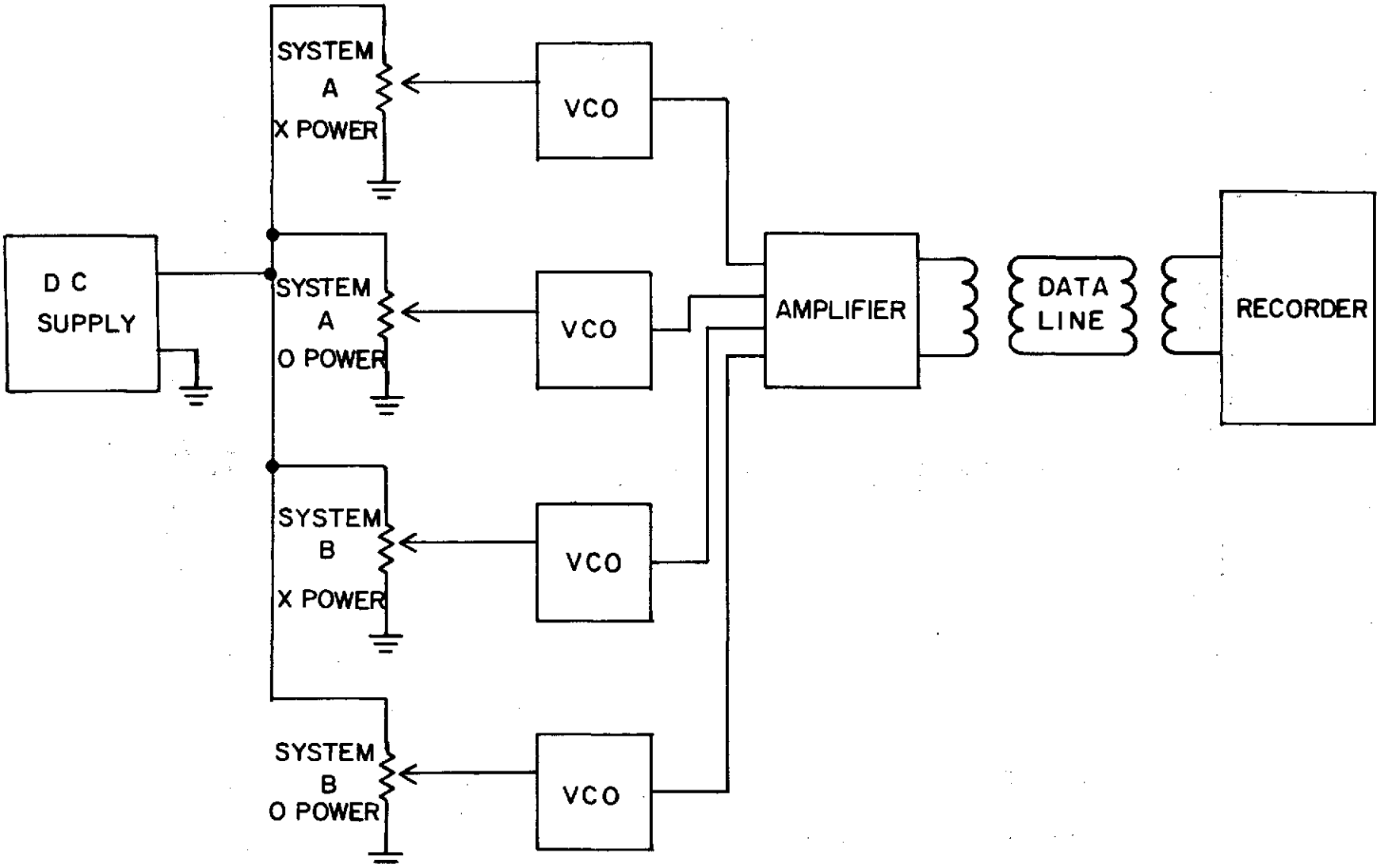

Figure 3.2 Block diagram of frequency modulated data link.

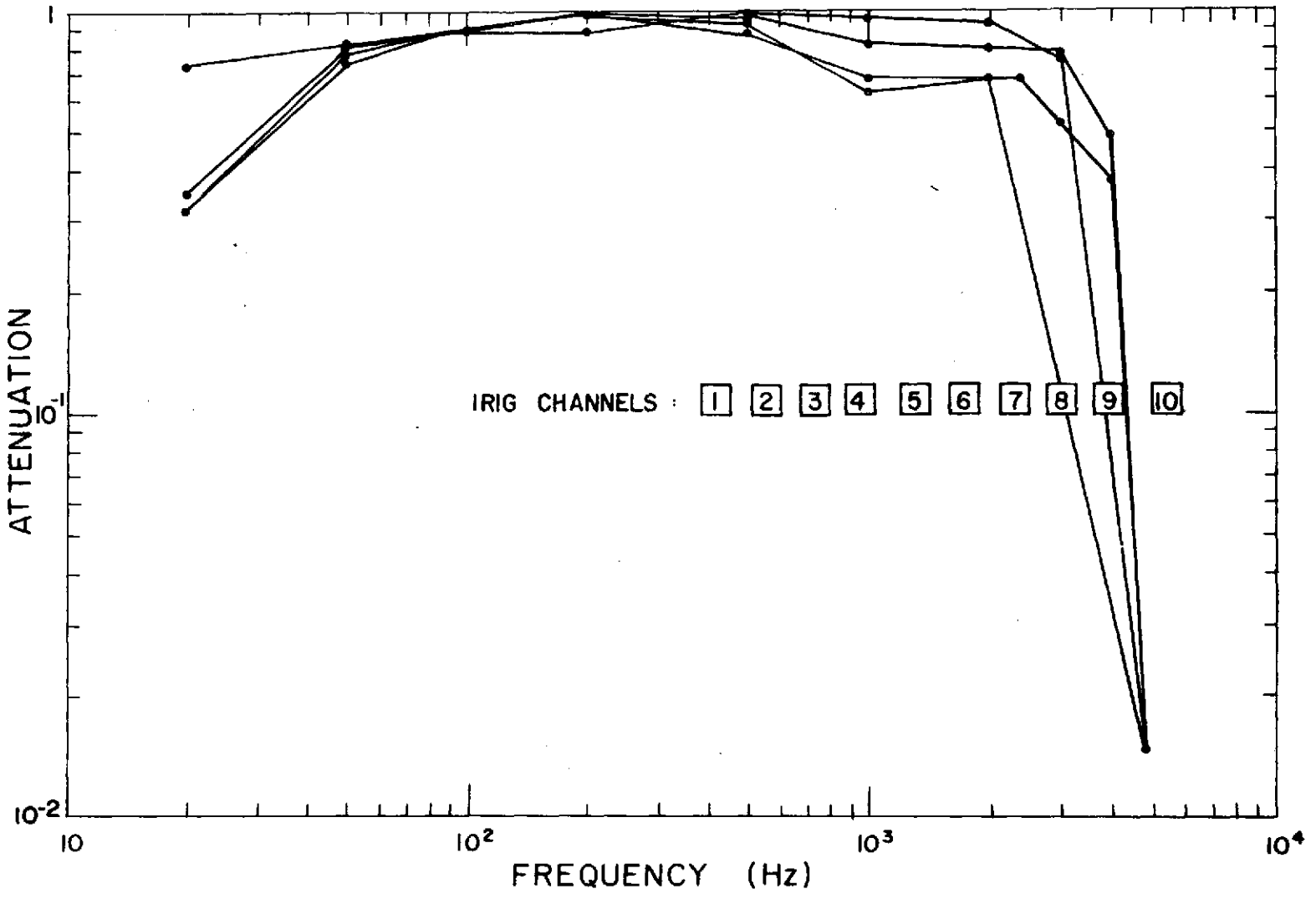

Figure 3.3 Measured frequency response of four data lines at Wallops Island, shown in relation to IRIG channels 1 to 10.

3.1.3 *Data reduction with frequency modulated system.* As noted in Chapter 2, with the addition of the FM system, the process of digitization is simplified since the additional rectifier in Figure 2.6 is no longer required. The change from the AM to the FM system, however, revealed an inefficiency in the median value subroutine of DAPROC.

When 14.511, the first rocket launch during which the FM system was used, was processed it took DAPROC four minutes of IBM 360 computer time to analyze 4 seconds of data, where previously up to 40 seconds had been processed when the AM system was employed. To show how this happened, Figures 3.4 and 3.5 show how samples of data for both the AM and FM system might look. The noise present in the AM system is a function of two factors: 1) increase noise in data transfer, and 2) incomplete filtering of the carrier signal by the rectifier.

If the signal has no noise and the curve is monotonically increasing, the median value will be located at the mid-point on the time axis of the period of interest. With the noisy data, the routine would find the median in a reasonable time because a point of magnitude equal to the median is found early in the data. If the data are smooth, as that generated by the FM system, the routine will search through nearly half the data to get to the median. With 10,000 data points, this means 5,000 passes through the data making comparisons, or 5×10^7 comparisons.

To rectify the problem, the statement directly above 200 in DAPROC, Figure 3.6, is changed to Test = XPWR(ISTOP/2), moving the initial search point to the mid-point of the time slot. With this change, DAPROC was able to process 40 seconds of data from 14.511 in less than three minutes.

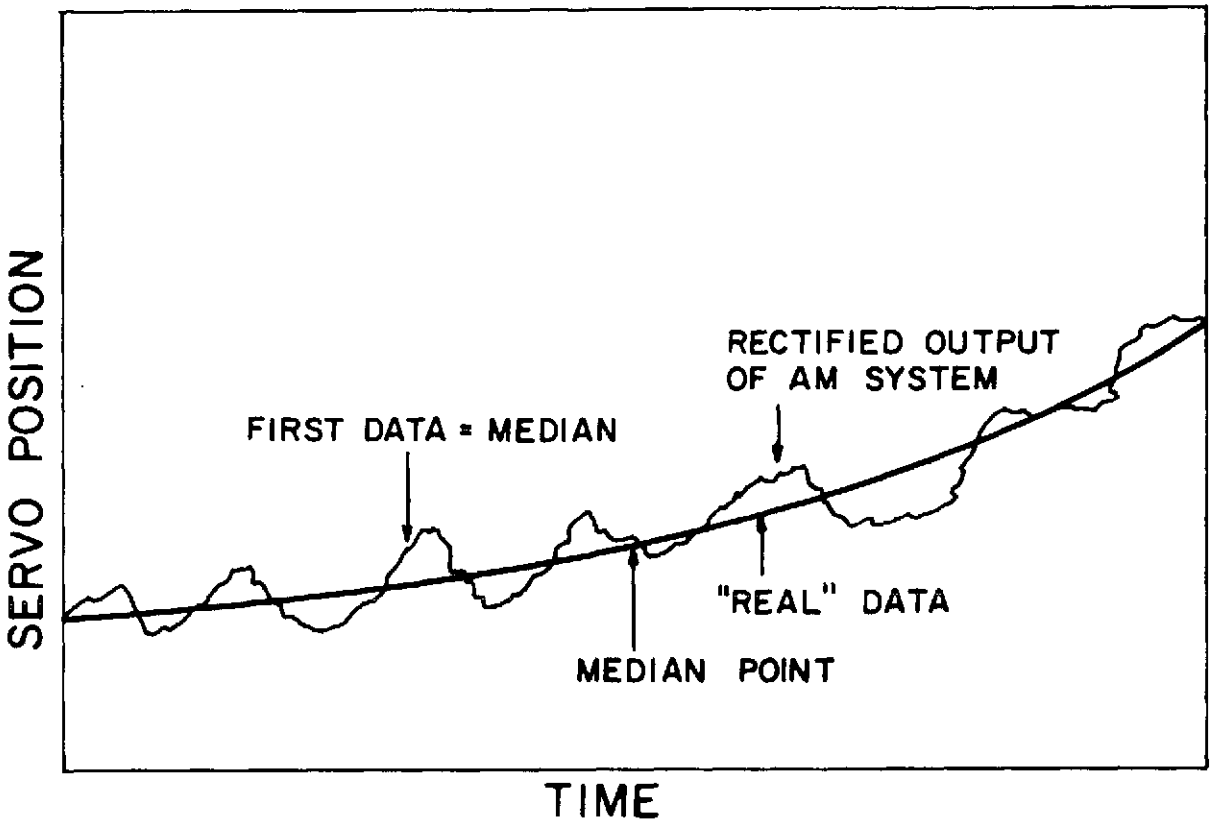

Figure 3.4 Possible AM system data.

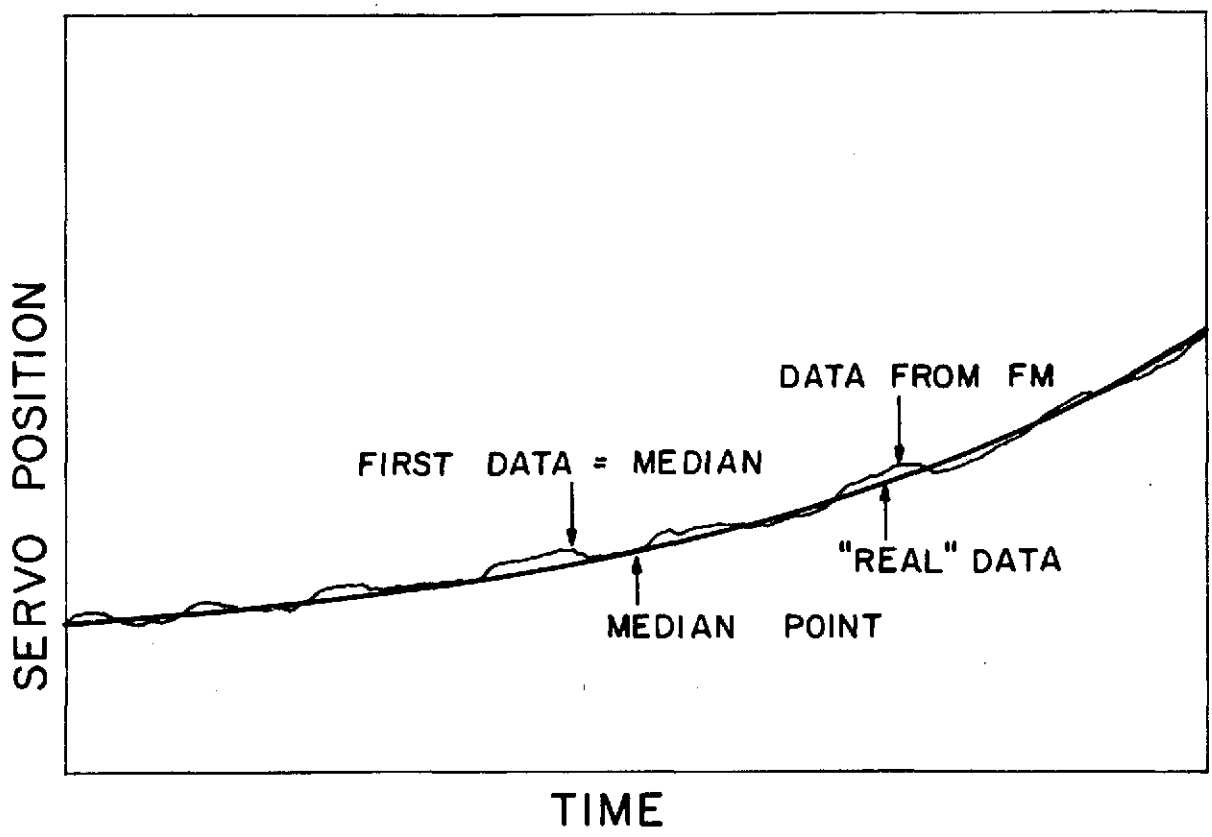

Figure 3.5 Possible FM system data.

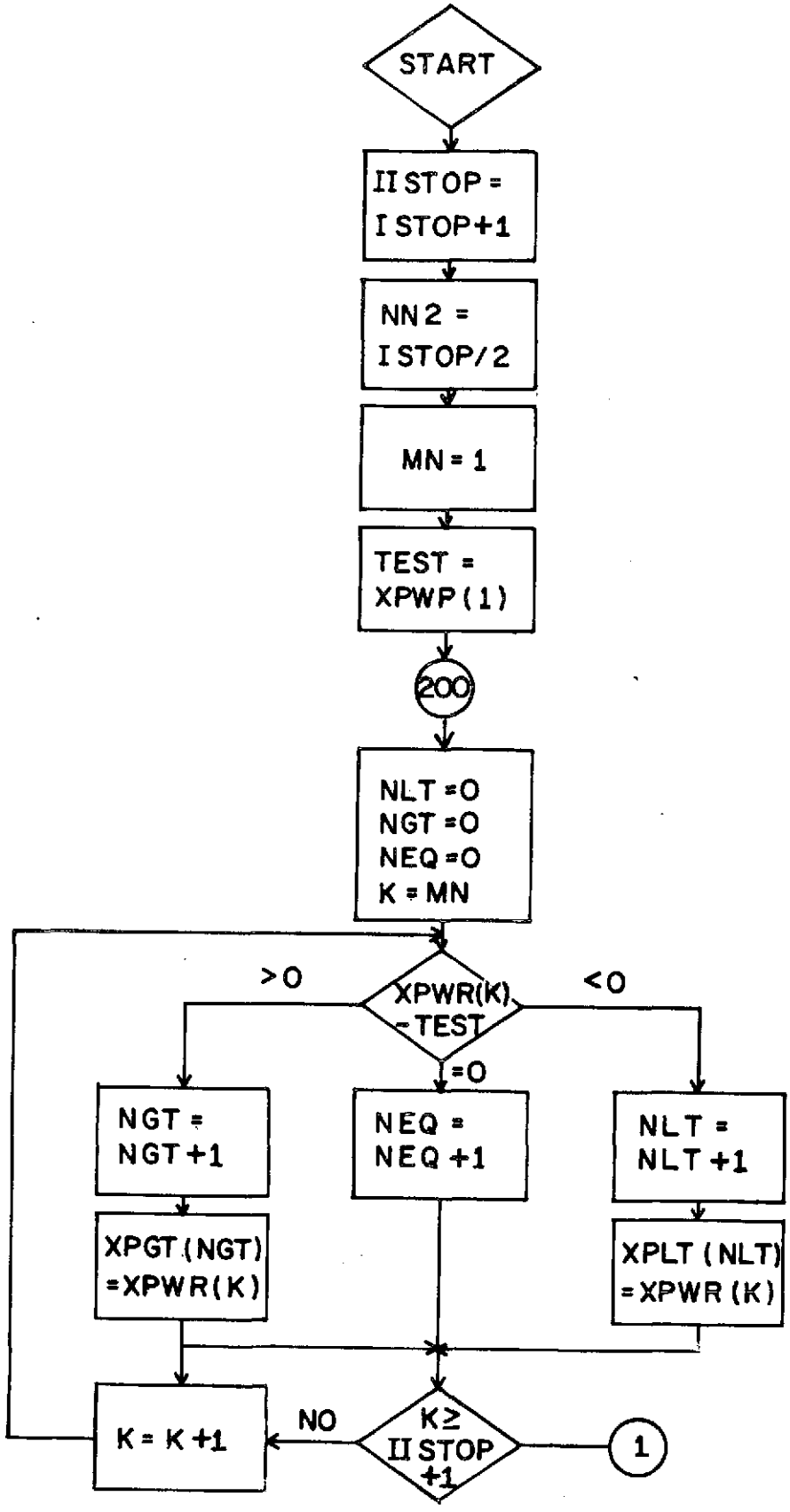

Figure 3.6 Flowchart of original DAPROC program. This flowchart is a corrected version of that given by *Slekys and Mechtly* [1970]. The program listing in that reference is correct and is currently stored on the IBM 360.

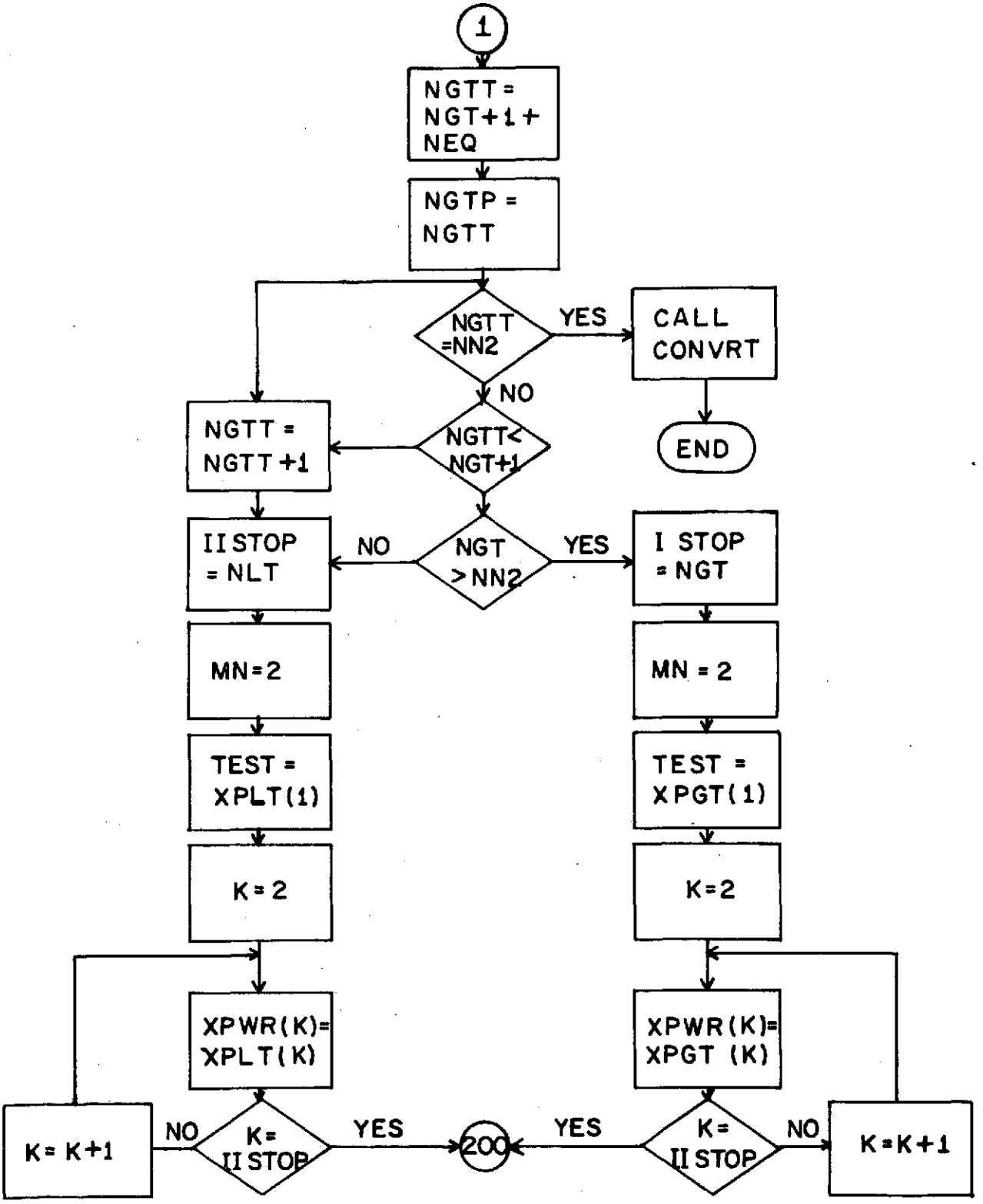

Figure 3.6 Continued

3.1.4 *Verification of data link improvement by use of FM system.* As a means of testing the improvement made by using the FM system, data, digitized while the potentiometers at the University of Illinois van were locked, were analyzed as if it represented real data. Table 3.1 lists the rates of differential absorption that resulted from noise in the systems. (During this test tape speed compensation discussed later was employed.) The standard error of the FM system is .006 dB/sec with a maximum change of .01 dB, the minimum change the programs are designed to measure. The older AM system showed a larger .037 dB/sec standard with errors up to .09 dB/sec possible.

As a result of the FM system, the data transfer can be eliminated as a factor in the overall noise of the measurements involved in the differential absorption experiment.

3.2 *Effects of Tape Speed Variation on Data and its Correction*

Figure 3.7 shows a chart record of the output of a discriminator after being passed through a low pass filter of 10 Hz to remove the real data, which are on a carrier at 145 Hz. What this signal represents is tape speed noise caused by flutter in the tape playback system.

In the analysis of data one second of data at a time has been used in most cases. If the tape speed noise is assumed periodic, the worst case occurs when one second of data corresponds to a multiple of the period of the noise plus a half period,

$$1 \text{ sec} = NT + T/2$$

TABLE 3.1

Test of Data Transfer System

Referenced Time	D.A. Rate in dB/sec AM system	FM system
1	-.02	0
2	-.09	-.01
3	-.04	0
4	0	.01
5	.02	0
6	0	0
7	.02	0
8	0	0
9	0	0
10	-.04	0
11	.07	0
12	.02	0
13	-.02	-.01
14	0	.01
15		0
16		.01
17		-.01

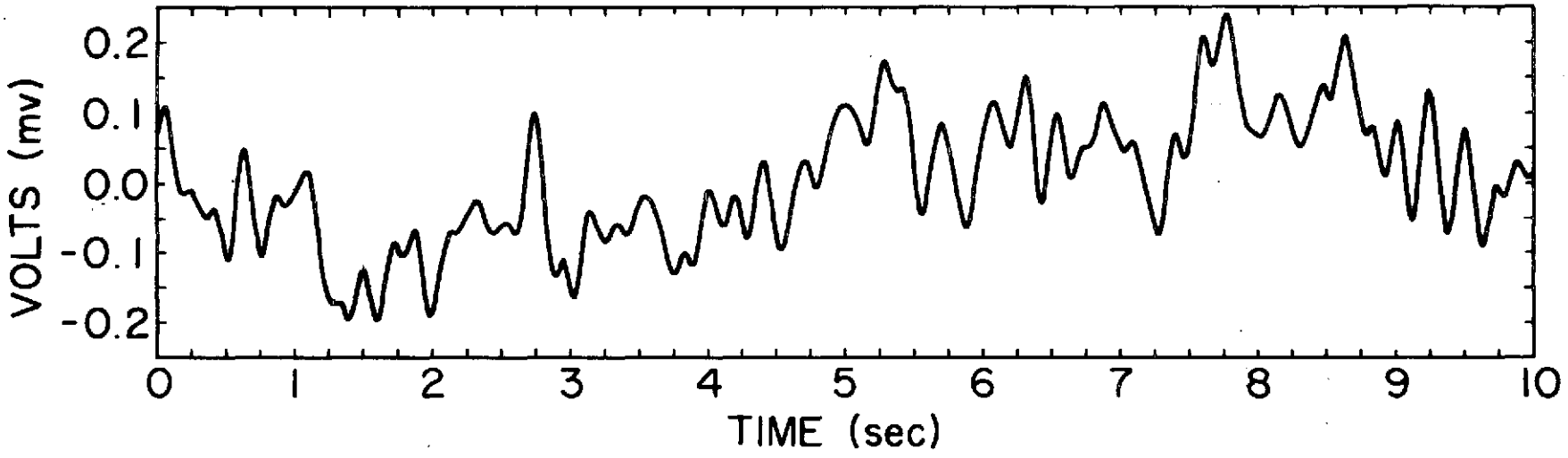

Figure 3.7 Tape Speed Error.

Under this condition, the total error caused by a signal of frequency f and amplitude A is

$$\text{Error} = \frac{A}{2\pi f}$$

in the one second of data. Since two adjacent seconds are used to compute differential absorption rates and their errors will be in opposite directions, the error in measurement will amount to

$$\text{Error} = \frac{A}{\pi f} .$$

The noise in Figure 3.7 was found to have a primary frequency of about 3.5 Hz and amplitude of .4 dB, so the resulting error would be .02 dB.

3.2.1 *Implementation of tape speed compensation.* In order to compensate for variation in the speed of tape passing through the playback system, tape speed compensation was implemented. TSC operates by recording a 100 KHz signal onto the data tape at the same time the data are recorded. During playback, this signal is fed into a reference discriminator centered at 100 KHz. The output of the discriminator is proportional to the difference between 100 KHz and the frequency of the signal from the tape.

The signal to be digitized is passed through a delay line and then into the discriminator. The delay line compensates for the time it takes the 100 KHz signal to be processed in the reference discriminator. The

normal output of the discriminator is then added to the signal from the reference. The resulting signal will have noise due to the tape speed variation reduced by 30 dB.

3.2.2 *Effectiveness of tape speed compensation in reducing noise.* To see what kind of improvement tape speed compensation would make, flight 14.514 was reprocessed both with and without TSC. Table 3.2 shows the results of these runs. The standard correction is ±.015 dB/sec. For a correction of this order, the 30 dB noise reduction of the TSC system is sufficient to reduce tape speed noise below the levels measurable by the programs.

3.3 *Filtering of Signals to be Processed from AM System to Improve Data*

Another test performed, to improve the quality of data processed for flights employing the AM system, involved the use of filtering. A bandpass filter is placed between the discriminator output and the rectifier in Figure 2.6. The filter will remove noise that is not associated with the data signal, such as dc offset noise. The results of this test for flight 14.361 are shown in Table 3.3. The correction has a standard value of .02 dB/sec. This is a small error relative to those seen in the data, and thus does not warrant reprocessing of older flights.

3.4 *Results of Improvements*

All of the new techniques discussed in this chapter have contributed in some way to the more exact evaluation of data, but none accounts for the large discrepancies noted in Chapter 1. Possible explanations for the larger errors are covered in the following chapter, along with errors that do not affect data at low altitudes but become important higher up in the ionosphere.

TABLE 3.2

Test of Tape Speed Compensation on Data from 14.514

TIME after launch	Differential Absorption Rates (dB/sec) TSC	no TSC	Difference TSC - no TSC
40	0	0	0
41	0	.02	.02
42	-.11	-.11	0
43	.08	.07	-.01
44	.05	.05	0
45	0	.02	.02
46	-.15	-.16	-.01
47	.10	.10	0
48	.13	.13	0
49	-.05	-.03	.02
50	.11	.11	0
51	.02	0	-.02
52	.02	.03	.01
53	0	0	0
54	.59	.57	-.02
55	.16	.16	0
56	.72	.70	-.02
57	1.12	1.16	-.04
58	1.25	1.25	0
59	2.34	2.33	-.01
60	3.09	3.09	0
61	2.86	2.88	.02
62	2.67	2.68	.01
63	2.49	2.53	.04
64	2.23	2.22	-.01
65	1.36	1.36	0
66	1.42	1.41	-.01
67	1.64	1.65	.01
68	1.45	1.44	-.01
69	1.13	1.12	-.01
70	-.02	-.03	-.01
71	-.08	-.06	.02
72	.32	.29	-.03
73	-.11	-.01	.02
74	.94	.92	-.02
75	1.02	1.01	-.01

TABLE 3.3

Filter Test on 14.361

Time after launch	Differential Absorption Rates (dB/sec) No Filter	Filter	Change
48	.16	.20	-.04
49	.48	.46	.02
50	-.11	-.11	0
51	-.36	-.37	.01
52	.40	.42	-.02
53	.39	.37	.02
54	-.28	-.28	0

4. ERRORS IN THE SIGNAL RECEIVED BY THE ROCKET

This chapter will deal with errors not connected with the processing or recording of data, but with errors at the rocket itself. The first two sections present a more detailed analysis of the electric field than has previously been undertaken and shows some faults in the experimental assumptions. The last section deals with actual errors in the receiving system itself.

4.1 *Theory of Polarization Errors*

The type of signals which can be expected from errors in the polarization, those due to imperfect generation of the extraordinary and ordinary modes, are examined. The wave form detected by the receiver was derived as follows.

Two signal components are considered to be present at the frequency $\omega - \delta$. They are the ordinary wave,

$$\hat{i}\, Q \sin[(\omega-\delta)t - K_{oo}Z] - \hat{j}\, Q \cos[(\omega-\delta)t - K_{oo}Z]$$

and the unwanted extraordinary wave,

$$\hat{i}\, S \sin[(\omega-\delta)t - K_{xo}Z] + \hat{j} \cos[(\omega-\delta)t - K_{xo}Z]$$

At the frequency $\omega + \delta$ there are also two components present. The extraordinary wave is represented as

$$\hat{i}\, R \sin[(\omega+\delta)t - K_{xx}Z] + \hat{j}\, R \cos[(\omega+\delta)t - K_{xx}Z]$$

and an unwanted ordinary wave is

$$\hat{i}\ P \sin[(\omega+\delta)t - K_{ox}Z] - \hat{j}\ P \cos[(\omega+\delta)t - K_{ox}Z]$$

The unit vector for the antenna is taken as in Chapter 2 to be

$$\hat{a} = -\hat{i}\ \sin\omega_r t + \hat{j}\ \cos\omega_r t \tag{4.1}$$

and the displacement is taken as

$$Z = v_R t \tag{4.2}$$

K_{oo}, K_{xo}, K_{xx}, and K_{ox} represent the propagation constants. The first subscript represents the mode of the wave, o for ordinary and x for extraordinary. The second subscript is the frequency of operation, o for the correct ordinary frequency $(\omega-\delta)$, and x for the correct extraordinary frequency $(\omega+\delta)$. v_r is again the rocket velocity and ω_r the spin rate of the rocket.

The signal received, represented as $\underset{\sim}{E} \cdot \hat{a}$ is

$$-[Q \sin(\omega-\delta-K_{oo}v_r)t + S \sin(\omega-\delta-K_{xo}v_r)t$$

$$+ R \sin(\omega+\delta-K_{xx}v_r)t + P \sin(\omega+\delta-K_{ox}v_r)t] \cdot \sin\omega_r t$$

$$+ [-Q \cos(\omega-\delta-K_{oo}v_r)t + S \cos(\omega-\delta-K_{xo}v_r)t$$

$$+ R \cos(\omega+\delta-K_{xx}v_r)t - P \cos(\omega+\delta-K_{ox}v_r)t] \cos\omega_r t$$

which is

$$- Q \cos(\omega-\delta-K_{oo}v_r-\omega_r)t + S \cos(\omega-\delta-K_{xo}v_r-\omega_r)t$$

$$+ R \cos(\omega+\delta-K_{xx}v_r+\omega_r)t - P \cos(\omega+\delta-K_{ox}v_r-\omega_r)t$$

This may be rewritten as

$$[- Q \cos(-\delta-K_{oo}v_r-\omega_r)t + S \cos(-\delta-K_{xo}v_r+\omega_r)t + R \cos(\delta-K_{xx}v_r+\omega_r)t$$

$$- P \cos(\delta-K_{ox}v_r-\omega_r)t] \cos\omega t + [Q \sin(-\delta-K_{oo}v_r-\omega_r)t - S \sin(-\delta-K_{xo}v_r+\omega_r)t$$

$$- R \sin(\delta-K_{xx}v_r+\omega_r)t + P \sin(\delta-K_{ox}v_r-\omega_r)t] \cdot \sin\omega t$$

or in complex notation as shown below

$$Re\{[-Q \cos(-\delta-K_{oo}v_r-\omega_r)t + S \cos(-\delta-K_{xo}v_r+\omega_r)t$$

$$+ R \cos(\delta-K_{xx}v_r+\omega_r)t - P \cos(\delta-K_{ox}v_r-\omega_r)t$$

$$-jQ \sin(-\delta-K_{oo}v_r-\omega_r)t + jS \sin(-\delta-K_{xo}v_r+\omega_r)t$$

$$+ jR \sin(\delta-K_{xx}v_r+\omega_r)t - jP \sin(\delta-K_{ox}v_r-\omega_r)t]e^{j\omega t}\}$$

The amplitude detected by the receiver is

$$\{Q^2 + S^2 + R^2 + P^2 - 2QS \cos[-(K_{oo}-K_{xo})v_r - 2\omega_r]t$$

$$-2QR \cos[-2\delta-(K_{oo}-K_{xx})v_r - 2\omega_r]t + 2QP \cos[-2\delta-(K_{oo}-K_{ox})v_r]t \qquad (4.3)$$

$$+2SR \cos[-2\delta-(K_{xo}-K_{xx})v_r]t + 2SP \cos[-2\delta-(K_{xo}-K_{ox})v_r + 2\omega_r]t$$

$$-2RP \cos[(K_{xx}-K_{ox})v_r + 2\omega_r]t\}^{1/2}$$

The relation

$$(1 + X)^{1/2} \simeq 1 + \frac{X}{2}$$

for X small may be used to reduce expression (4.3). Table 4.1 lists the resulting frequencies and their proportional amplitudes.

Each frequency can be given a physical interpretation to help understand what errors are occurring. Frequency b at $2\delta + 2\omega_r$ is the frequency discussed in Chapter 2. Frequencies a and f are caused by the error signals at each transmitted frequency combining with the correct signal to form a small linear signal. The linear signal's received strength is then dependent on the antenna orientation and is therefore modulated at $2\omega_r$. Frequencies e and d are both caused by signals of the same polarization, but different transmitter frequencies. Since they are the addition of two circular modes in the same direction, they result in a circular mode and are unaffected by rocket spin. The 2δ is caused by the envelope generated by the difference in frequency.

TABLE 4.1

Received Frequencies Including Polarization Errors

a	$(K_{oo}-K_{xo}) + 2\omega_r$	$2\omega_r$	QS
b	$2\delta + (K_{oo}-K_{xx})v_r + 2\omega_r$	$2\delta + 2\omega_r$	QR
c	$2\delta + (K_{oo}-K_{ox})v_r$	2δ	QP
d	$2\delta + (K_{xo}-K_{xx})v_r$	2δ	SR
e	$2\delta + (K_{xo}-K_{ox})v_r - 2\omega_r$	$2\delta - 2\omega_r$	SP
f	$(K_{xx}-K_{ox})v_r + 2\omega_r$	$2\omega_r$	RP
g	dc		$[P^2+Q^2+R^2+S^2]^{1/2}$

Frequency e is generated as in Chapter 2 but since the ordinary wave is now higher in frequency, the ellipse rotates opposite to the direction in Chapter 2 and the rocket spin thus subtracts from the total. The dc signal is the average signal strength present at the rocket.

4.2 *Effect of Polarization Errors on System Response*

Figures 4.1, 4.2, and 4.3 show the probe current and DA determined electron concentrations. Note that in all cases the DA data from the 2.225 MHz system indicate low electron densities above 80 km. To see if this could be due to polarization errors, a Fourier transform program developed by K. L. Miller [*Edwards*, 1973] was used to recover the power in the frequency components at 2δ, $2\delta + 2\omega_r$ and $2\omega_r$. These powers are shown in Figures 4.4 to 4.6. To see what has happened, it is assumed that the error extraordinary signal is negligible; thus, $S = 0$ in Table 4.1. The amplitude of the ordinary error signal, P, may not be assumed to be 0 since as the extraordinary wave is absorbed the power to the extraordinary transmitter is increased, and thus the power in the error wave, P. As the ratio of ordinary to extraordinary is being kept constant, the magnitude of the error ordinary signal continues to increase. At some point the magnitude of the error ordinary wave and the extraordinary wave at the rocket are equal. At this point, the servo system will follow the 2δ rad/sec signal generated by the two ordinary modes rather than the correct $2\delta + 2\omega_r$ rad/sec signal. Appreciable degradation of data is noted to occur when the 2δ rad/sec signal power reaches about one-fifth the magnitude of the $2\delta + 2\omega_r$ rad/sec component. To get a measure of how much useful data can be extracted from a flight, the powers of the 2δ and $2\delta + 2\omega_r$ components at low altitudes can be

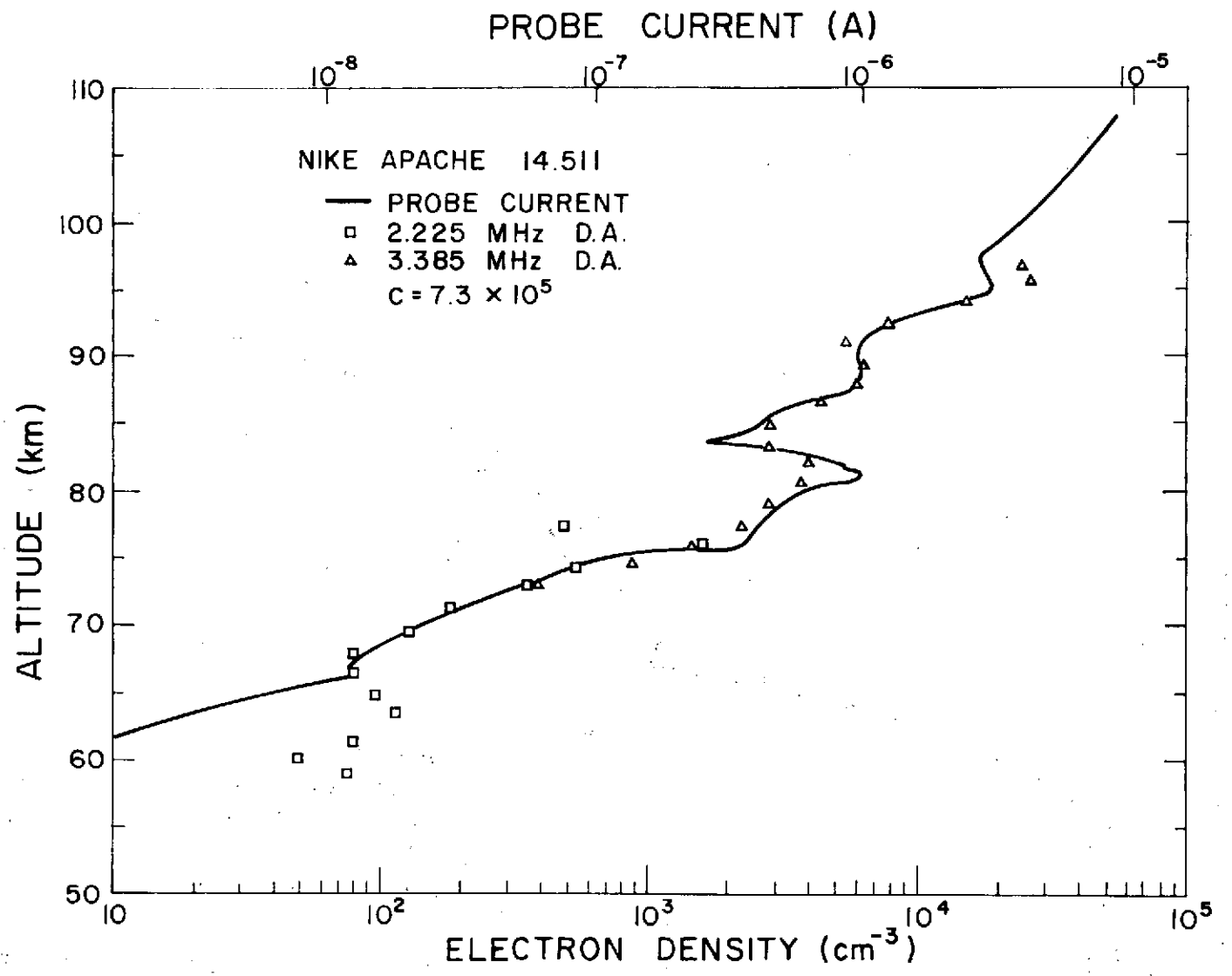

Figure 4.1 Profiles of probe current (upper scale) and electron density (lower scale). Data from the differential absorption experiment alone are shown.

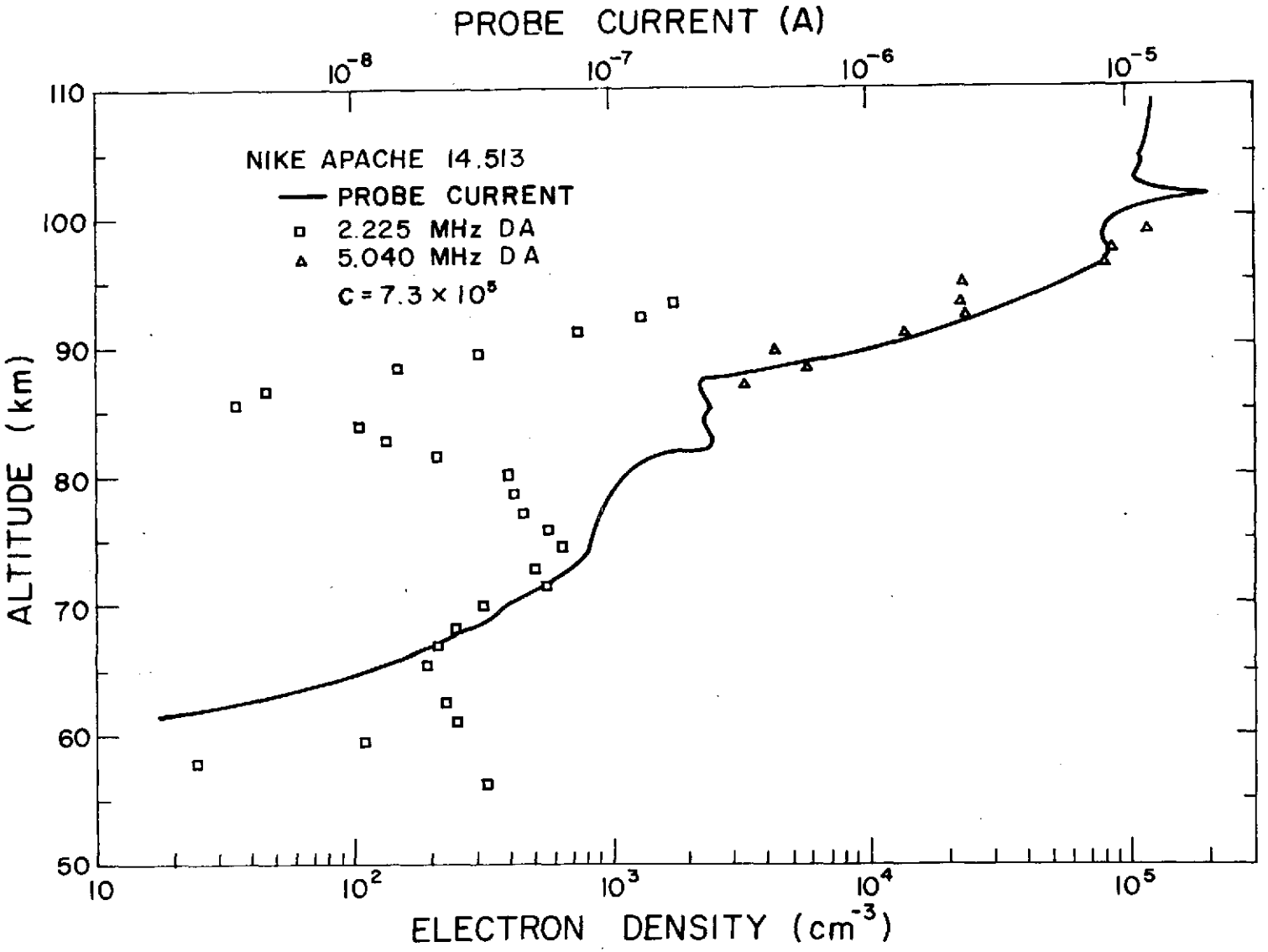

Figure 4.2 Profiles of probe current (upper scale) and electron density (lower scale). Data from the differential absorption experiment alone are shown.

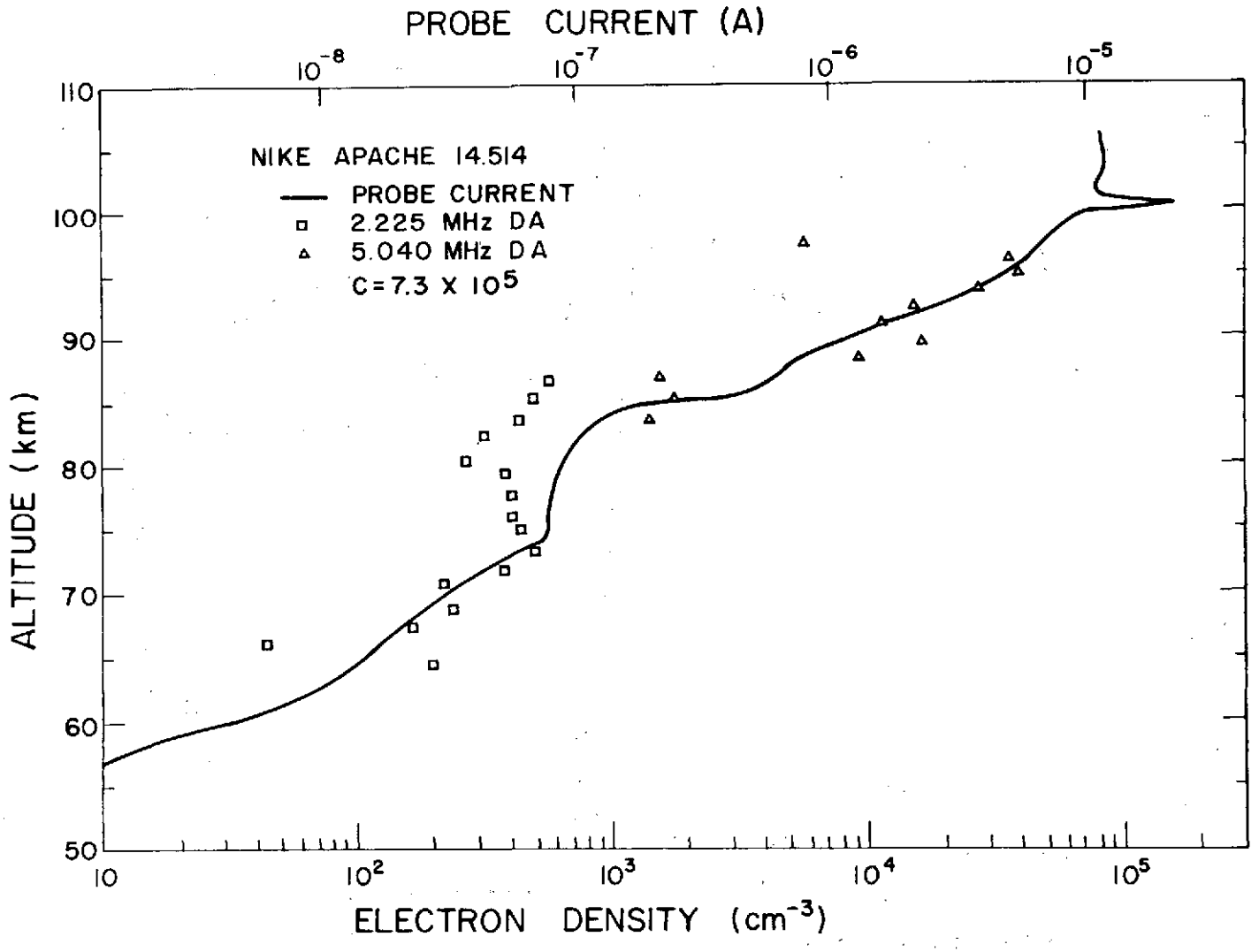

Figure 4.3 Profiles of probe current (upper scale) and electron density (lower scale). Data from the differential absorption experiment alone are shown.

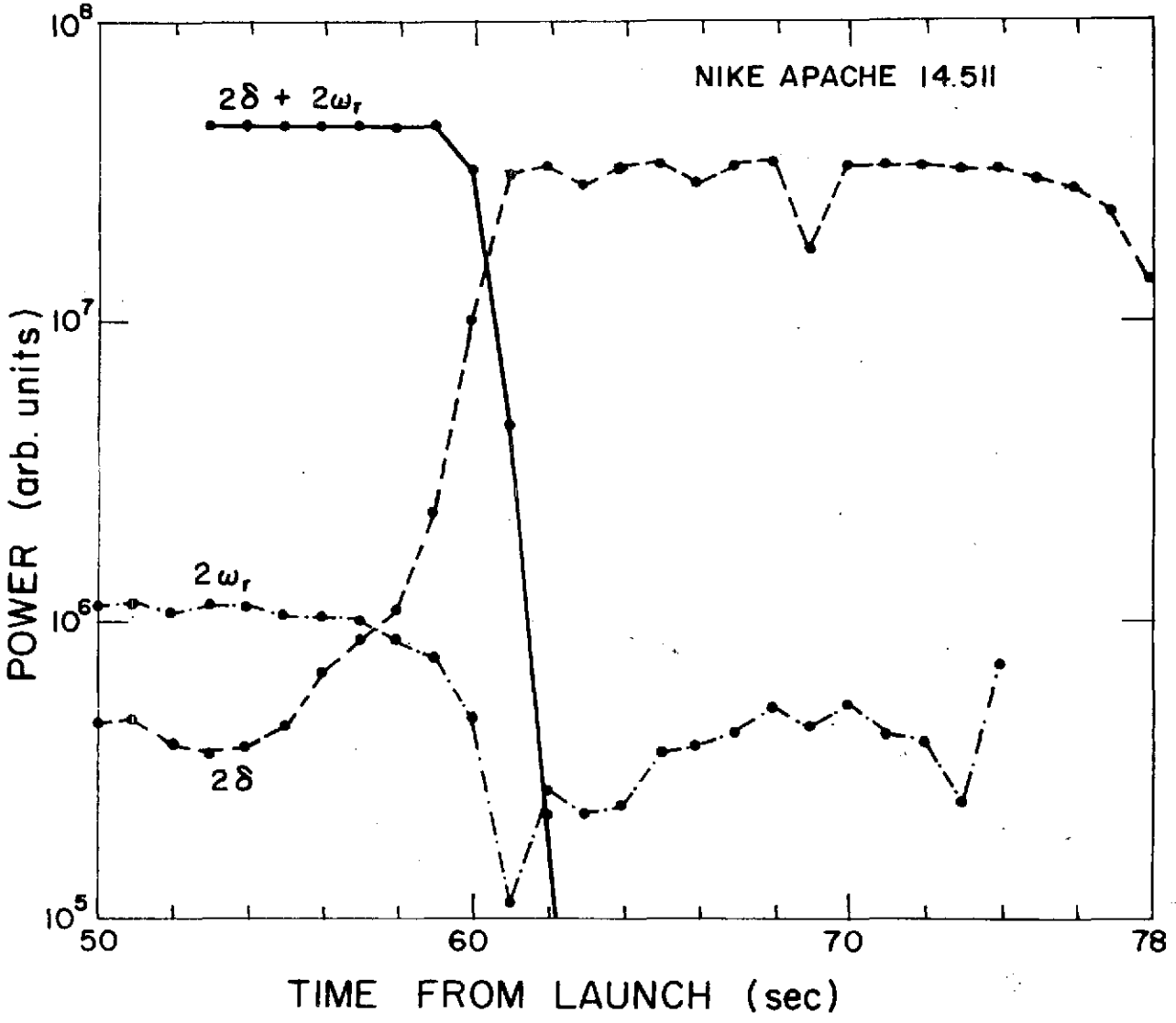

Figure 4.4 Frequency components at receiver output.

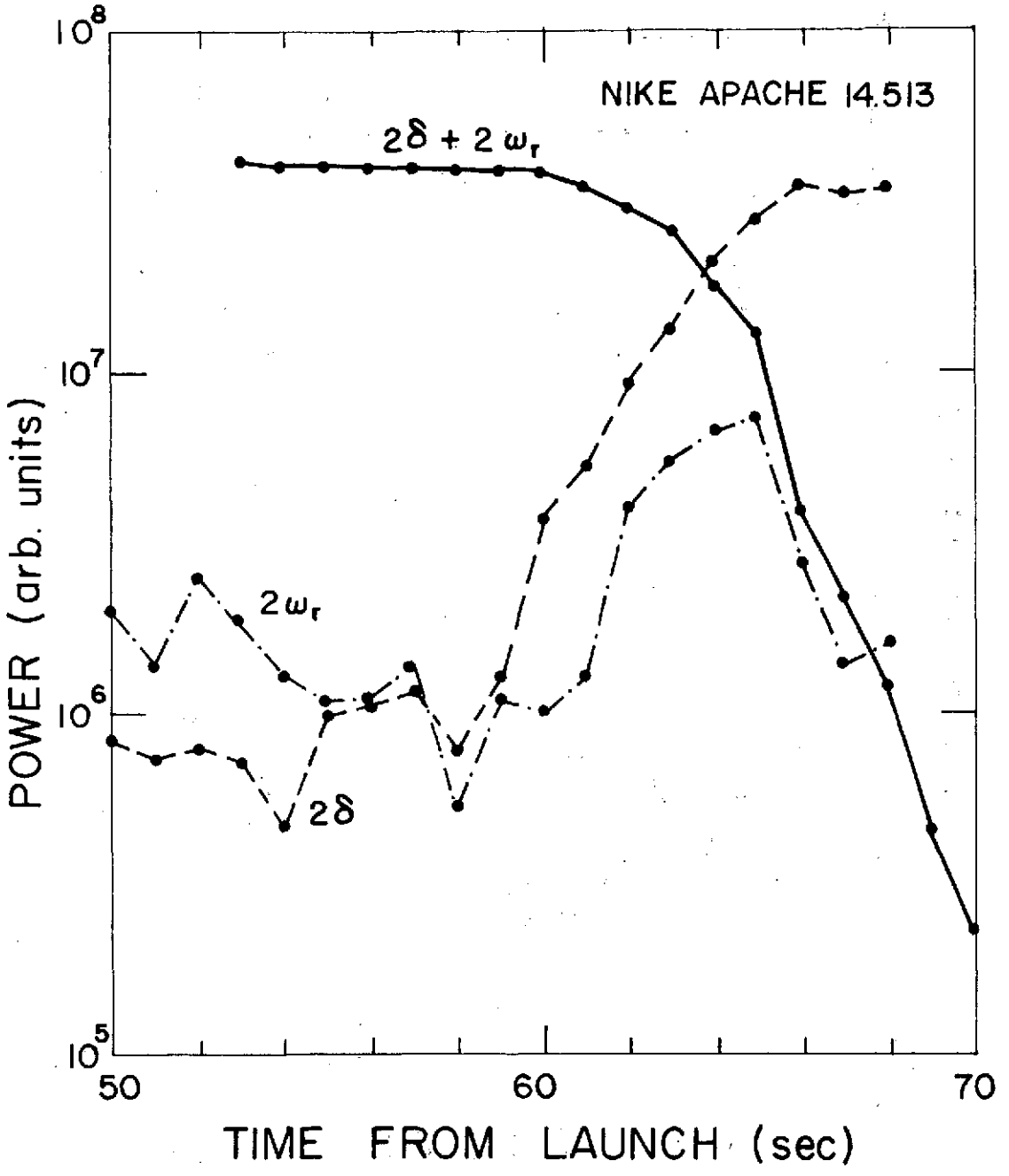

Figure 4.5 Frequency components at receiver output.

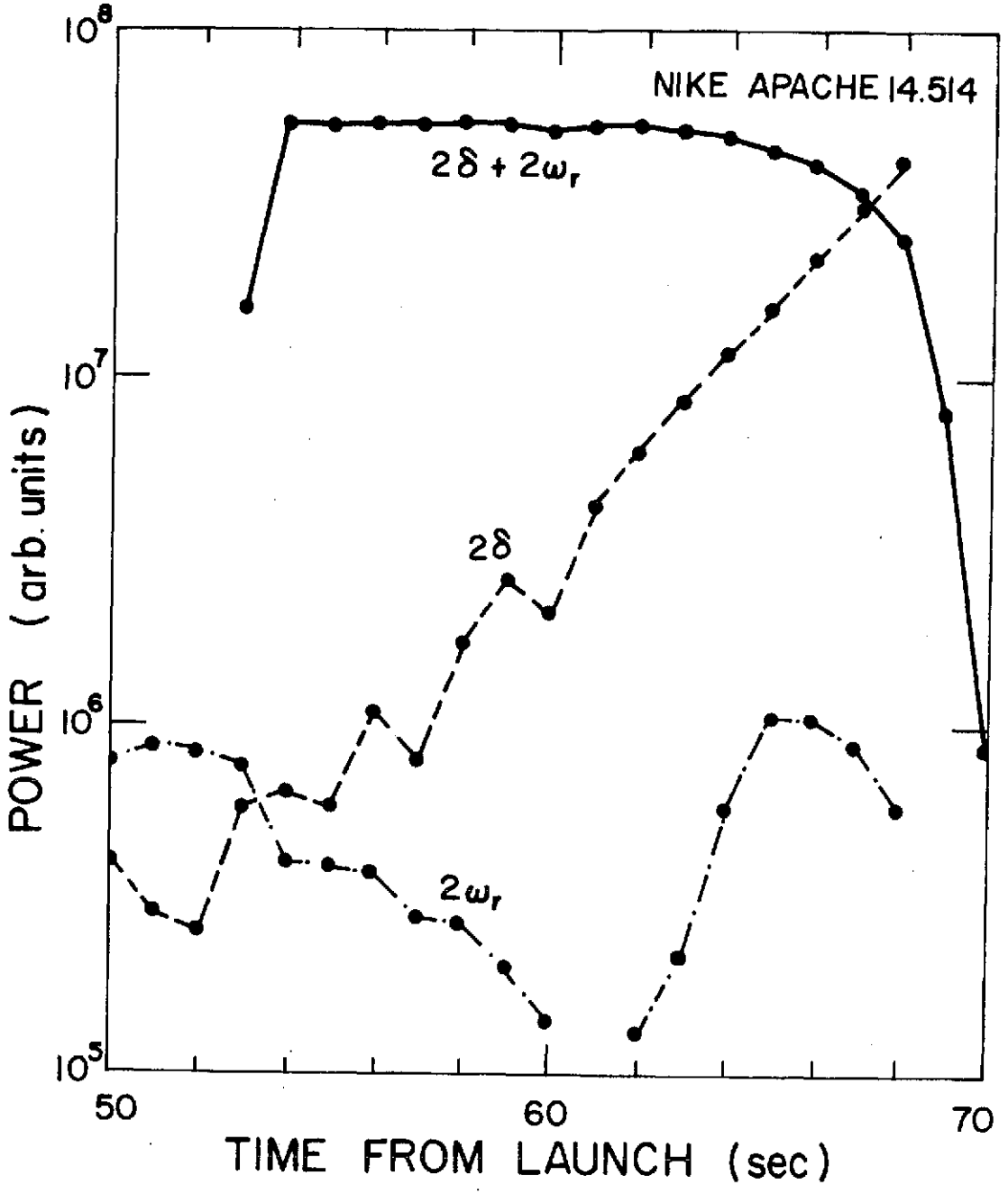

Figure 4.6 Frequency components at receiver output.

compared. The difference in power in decibles minus seven decibles gives the total range of useful absorption, the sum of the rates for each second. Table 4.2 lists the power differences and useful data range for 14.511, 14.513, and 14.514 and the second of flight and altitude where the limit is passed.

4.3 *Reflected Waves*

The following will give an idea of the error to be expected when reflections are present. The reflection coefficients for the extraordinary and ordinary waves, as measured from the rocket, may be represented as Γ_x and Γ_o. Since the reflection coefficients are measured from the rocket, they include absorption over the path of the reflected wave. The propagation will be along a magnetic field line so that the mode of the reflected wave is the same as that of the incident wave. The error in polarization is assumed to be zero.

The total electric field may be calculated as the sum of four propagation vectors. First there are the two upward propagating modes

$$\hat{i}Q \sin[(\omega-\delta)t - KZ] - \hat{j}Q \cos[(\omega-\delta)t - KZ]$$

and

$$\hat{i}R \sin[(\omega+\delta)t - KZ] + \hat{j}R \cos[(\omega-\delta)t - KZ]$$

where it is now assumed for simplicity that the propagation constant, K, is the same for both modes. The two reflected vectors can be represented as

$$\hat{i}Q\Gamma_o \sin[(\omega-\delta)t + KZ] - \hat{j}Q\Gamma_o \cos[(\omega-\delta)t + KZ]$$

TABLE 4.2

Power Differences, Useful Data Range, and Limit of Data in Time and Altitude for Three Rocket Flights

Flight	Difference Power (dB)	Useful Range (dB)	Last Useful Data Time (sec)	Last Useful Data Altitude (km)
14.511	20	13	59	75
14.514	19	12	61	75
14.513	19	11	59	75

and $\quad \hat{i}R\Gamma_o \sin[(\omega+\delta)t + KZ] + \hat{j}R\Gamma_x \cos[(\omega-\delta)t + KZ].$

By going through the procedure of Section 4.1 the amplitude of the signal detected by the receiver is

$$\{[1 + \Gamma_o^2]Q^2 + [1 + \Gamma_x^2]R^2 - 2QR \cos(2\delta + 2\omega_r)t$$

$$+ 2Q^2\Gamma_o \cos(2Kv_r)t - 2QR\Gamma_x \cos[2\delta + 2Kv_r + 2\omega_r)t$$

$$- 2QR\Gamma_o \cos(2\delta - 2Kv_r + 2\omega_r)t$$

$$+ 2R^2\Gamma_x \cos(2Kv_r)t - 2QR\Gamma_o\Gamma_x \cos(2\delta + 2\omega_r)t\}^{1/2}.$$

If Γ_x and Γ_o are small and R is much less than Q the expansion used in Section 4.1 is valid and the amplitude and frequencies present in the output are shown in Table 4.3. Thus, under the conditions of reflected waves with absorption the modulation index, M, is

$$M = \frac{QR(1 + \Gamma_o\Gamma_x)}{[(1 + \Gamma_o^2)Q^2 + (1 + \Gamma_x^2)R^2]^{1/2}} \tag{4.4}$$

It can be seen that changes in the shape of the ionosphere above the rocket will cause the index M to change and the system to wander looking for a proper setting to hold M constant, as shown in Figure 4.7.

When perfect reflections occur the expansion used breaks down. To examine this case let $R = 0$, so that only the ordinary wave is present, and let $\Gamma_o = -1$. The receiver output is then

TABLE 4.3

Frequencies in Receiver Output when Reflections are Present

for $\Gamma_x, \Gamma_o \ll 1$ and $R \ll Q$

Frequency	Amplitude
dc	$[(1+\Gamma_o^2)Q^2 + (1+\Gamma_x^2)R^2]^{1/2}$
$2Kv_r$	$\Gamma_o Q^2 + \Gamma_x R^2$
$2\delta + 2\omega_r$	$QR + \Gamma_o \Gamma_x QR$
$2\delta + 2\omega_r + 2Kv_r$	$\Gamma_x QR$
$2\delta + 2\omega_r - 2Kv_r$	$\Gamma_o QR$

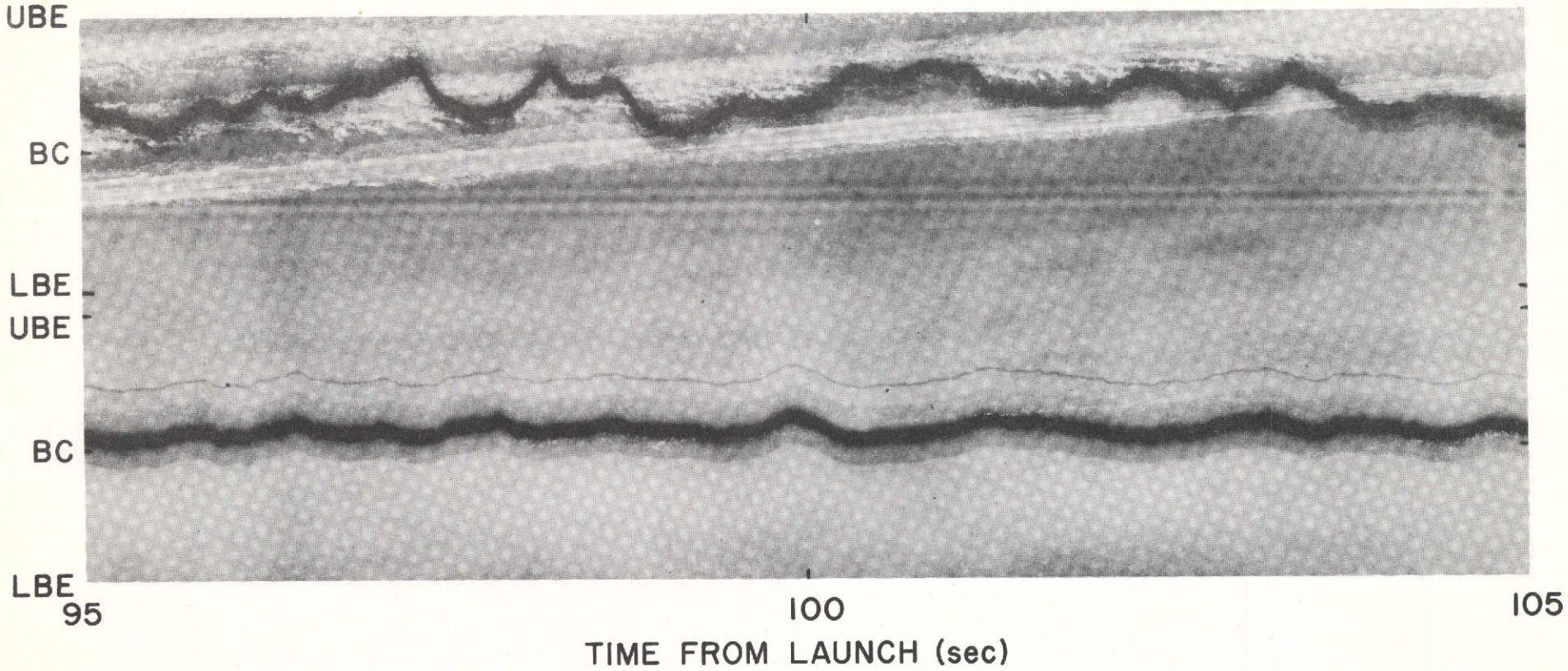

Figure 4.7 Section of chart record for Nike Apache 14.520 showing differential absorption signals in relation to lower band edge (LBE), band center (BC) and upper band edge (UBE). This is the FM system used for a nighttime flight.

$$[2Q^2 - 2Q^2 \cos(2K\upsilon_r t)]^{1/2}$$

This can be rewritten as

$$2Q|\sin(K\upsilon_r t)|$$

The frequencies in the output are shown in Table 4.4. Note that the dc term is larger than that for only an upward traveling ordinary wave when it would be simply Q.

It should be noted that this analysis does not hold near the ordinary reflection point the wave is no longer circular, but linear. Also the reflection occurs at $X = 1$ due to ray bending.

To connect the results of sections one to three of this chapter Figure 4.8 shows the output spectrum of the receiver during flight 14.270. All of the frequency components around 500 Hz predicted are present.

4.4 *Receivers*

Another source of errors in the experiment is the noise picked up by the receivers. Figure 4.9 shows the noise temperature, a measure of the amount of noise present, as a function of frequency. As can be seen, the frequencies used by the experiment, 2.225 KHz, 3.385 KHz, and 5040 KHz, are in a portion of the spectrum with highly variable noise characteristics. The following is a calculation of the signal-to-noise ratio at the rocket for the 2.225 KHz system.

The loss of signal due to the length of the propagating path for an isotropic radiator is

TABLE 4.4

Receiver Output for $\Gamma_o = -1$ and $R = 0$

Frequency Component	Altitude
dc	$\frac{4Q}{\pi}$
$2Kv_r$	$\frac{4Q}{3\pi}$
$4Kv_r$	$\frac{4Q}{15\pi}$
$2nKv_r$	$\frac{4Q}{(4n^2-1)\pi}$

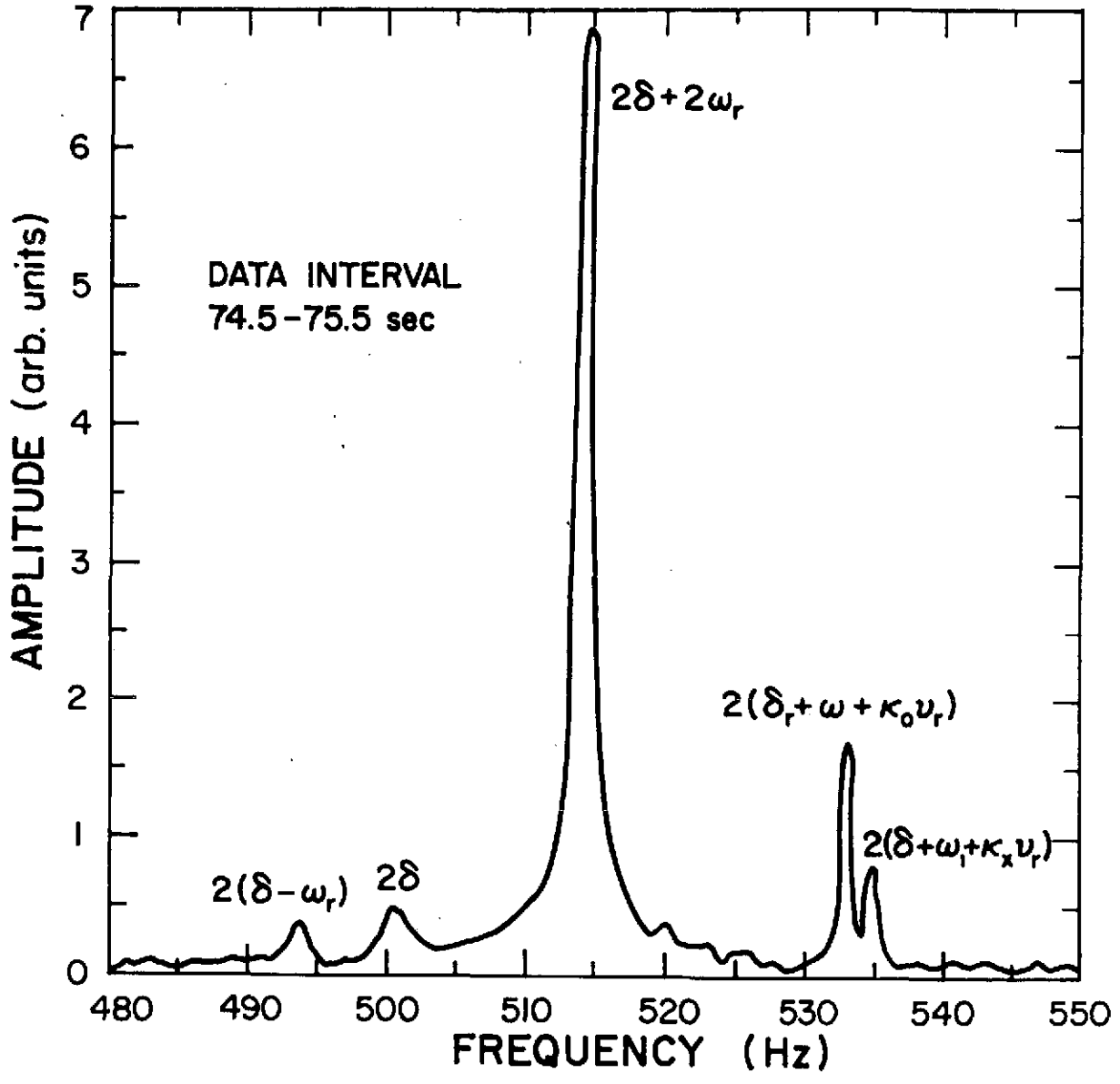

Figure 4.8 Frequency spectrum of receiver output signal for Nike Apache 14.270, prepared by K. L. Miller [*Edwards*, 1973].

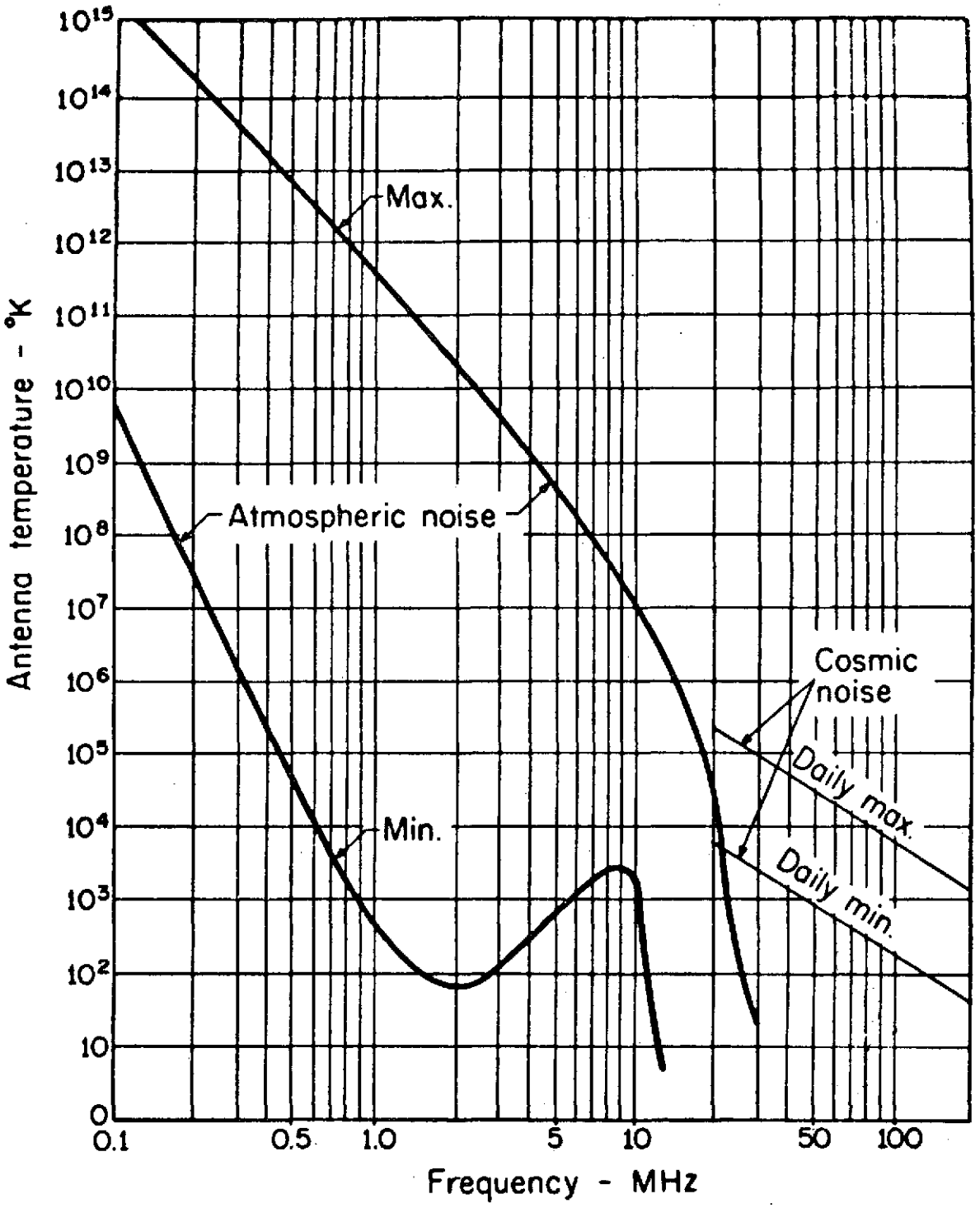

Figure 4.9 Noise temperature at medium and high frequencies [*Jordan and Balmain*, 1968].

$$L = 10 \log \frac{4\pi x h}{\lambda} \tag{4.5}$$

under the assumption of no absorption. If the rocket is at 100 km, the loss is 50 dB at 2.225 KHz. The transmitter power (P_T) is originally about 5 watts for the extraordinary signal which is 7 dBw. The combined gains of the antennas (G) are about 2 dB. The resulting signal power at the rocket is then

$$P_R = P_T + G - L \tag{4.6}$$

which is -41 dB in this case.

The total noise power received is

$$N = K' + T + B \tag{4.7}$$

in which K' is 10 log k (Boltzmann's constant), equal to -229 dBw/°K Hz, T is 10 log T_a (noise temperature) and B is 10 log BW (bandwidth). For a good payload receiver, BW is 1500 Hz. The temperatures chosen from Figure 4.10 are about 100°K at minimum and 10^{10}°K at maximum. These result in a maximum noise power of -100 dB and a minimum of -180 dB.

Comparing the signal power to the noise power, the signal-to-noise ratios of 139 dB and 59 dB result. Clearly random atmospheric noise is not an important factor over the 30 dB range of absorption the experiment is designed to operate over.

In addition to random atmospheric noise the signal may include unwanted radiofrequency transmissions. The receiver's bandpass

characteristic is poor in this respect. Examination of bandpass curves of receivers used in the payload shows a slow falloff and extraneous peaks. This can become important when the frequencies of the experiment are not far removed from those used by others. 2225 KHz is located in a frequency range used for radiotelegraph and ship-to-shore communications. Both of the upper frequencies used are within the tropical broadcast bands, used by countries near the equator because of poor propagation at normal broadcast band frequencies, as listed in Tables 4.5 and 4.6. Part of the hazard presented by these other users can be reduced by monitoring the receiver output prior to launch with the transmitters momentarily shut off. If there are any strong signals present, the rocket should not be launched unless poor performance of the differential absorption experiment is risked.

Another area in which other users of the airways may present a problem occurs because the receivers, when placed in a payload, receive signals at frequencies other than those for which they are designed. Table 4.7 shows the location of peaks outside the passband and the amount of attenuation at these points. It must be pointed out that this is not a particularly bad receiver and that all units tested showed this type of response. The frequency locations of these peaks do vary between receivers. Several of these fall in the broadcast band and if there is a nearby station it could affect data. This problem will show itself, if the above test for other stations near the operation frequency is done.

TABLE 4.5

Stations Near 3.385 MHz

Frequency	Power in Kilowatts	Country
3380	18	Mali
	100	Malawi
	1	Guatamala
	.25	Bolivia
	1	Peru
3385	.075	Indonesia
	.3	Indonesia
	10	Sri Lanka
	.6	New Guinea
	4	Dominican Republic
	1	Brazil
	1	Peru
	1	Venezuela
3390	10	Afghanistan
	120	China
	.2	Panama
	.25	Bolivia
	5	Ecuador
	.3	Peru

TABLE 4.6

Stations Near 5.040 MHz

Frequency	Power	Country
5037	1	Angola
	50	USSR
	30	Central African Rep.
	1	Brazil
	1	Columbia
	5	Ecuador
	.5, 1	Peru
5038	30	Central African Rep.
5039	20	Sudan
5040	50	USSR
	50	Burma
	none given	China
	.05	Indonesia
	.15	Haiti
	1	Ecuador
	10, .5	Peru
	1	Venezuela
5041	10	Guinea
	1	Phillipines
	1	Cook Islands
	5	Bolivia
	1	Brazil
	1	Peru

TABLE 4.7

Extra Signals Detected by

Receiver #106 in 5040 Payload

Frequency	Attenuation
556	-26 dB
585	-52 dB
601	-52 dB
635	-52 dB
674	-52 dB
695	-52 dB
741	-30 dB
856	-46 dB
927	-47 dB
1112	-23 dB
1236	-47 dB
1309	-43 dB
1483	-34 dB
1853	-42 dB
2780	-38 dB
3177	-28 dB
3705	-54 dB
4449	-20 dB

5. RANGE AND ACCURACY OF DIFFERENTIAL ABSORPTION DATA

In view of what has been discussed in the previous chapters about errors, it is appropriate to define a basis upon which the useful range of data may be determined. Chapter 4, Section 2, established an upper limit on the experiment, as a result of the polarization error. Here the lower limit of useful data will be fixed and some discussion of the accuracy of the measurements will be undertaken. For this purpose, Tables 5.1 to 5.3 present a summary of the results of the rate recovery program for three flights.

5.1 *Lower Limit of Differential Absorption Data*

The problem is to estimate the lowest differential absorption rate which can be considered to be a significant measure of real absorption. To get a measure of the random errors, several seconds of data are processed before absorption starts. This is then used to compute the standard error of measurement. Table 5.4 shows the errors for the flights under discussion. The criteria for determining the starting point for good data is to select the first data point greater than the standard error after which there are two or more data points also greater than the standard error. This point up to where polarization error takes over is the range of useful data.

Figures 5.1 to 5.3 show the probe current and only the useful differential data set by the procedures above and in Chapter 4. The polarization was not checked for the higher frequency in each experiment so the cutoff is taken as the first data point of value less than the standard error.

TABLE 5.1

14.511 - 2.225 and 3.385 KHz
Differential Absorption Rates

Time after launch	2.225 rate (dB/sec)	3.385 rate (dB/sec)
49	.07	.04
50	.05	-.19
51	.13	.27
52	.25	.27
53	.27	-.26
54	.27	.36
55	.33	.45
56	.60	.04
57	.96	-.35
58	1.79	.89
59	3.06	.92
60	8.49	2.07
61	2.39	2.75
62	.22	2.25
63		2.78
64		2.56
65		.73
66		.91
67		1.26
68		1.12
69		.62
70		1.42
71		.02
72		1.31
73		1.73
74		2.10
75		-1.16
76		1.34
77		.30
78		-.46
79		.62
80		.11

TABLE 5.2

14.513 - 2.225 and 5.04 MHz
Differential Absorption Rates

Time after launch	2.225 MHz (dB/sec)	5.04 MHz (dB/sec)
40	.12	
41	.10	
42	.04	
43	-.08	
44	.02	
45	.10	
46	-.04	
47	-.04	
48	.20	
49	.02	
50	.12	.18
51	.36	.18
52	.44	-.71
53	-.12	.37
54	.58	-.16
55	.74	-.05
56	1.04	.27
57	1.56	.16
58	2.96	.38
59	2.84	.07
60	3.70	-.05
61	3.21	.49
62	2.53	.02
63	2.10	.18
64	1.73	.22
65	.79	-.02
66	.42	-.05
67	.26	.75
68	.07	-.51
69	.07	.42
70	.31	.33
71	.52	-.18
72	.57	.58
73	.83	.47
74	.87	.37
75		.47
76		1.30
77		.84
78		.82
79		1.57
80		13.75
81		-.68
82		1.33

TABLE 5.2

14.513 - 2.225 and 5.04 MHz (cont.)

Time after launch	2.225 MHz (dB/sec)	5.04 MHz (dB/sec)
83		.12
84		-.20
85		-.27
86		-.88
87		4.56
88		-1.25
89		1.75
90		-2.58

TABLE 5.3

14.514 - 2.225 and 5.04 MHz
Differential Absorption Rates

Time	2.225 MHz (dB/sec)	5.04 MHz (dB/sec)
42	-.11	
43	.07	
44	.05	
45	.02	
46	-.16	
47	.10	
48	.13	
49	-.03	
50	.11	-.05
51	0	.02
52	.03	.47
53	0	-.46
54	.57	-.20
55	.16	-.07
56	.70	.38
57	1.16	.24
58	1.25	.02
59	2.33	-.15
60	3.09	.07
61	2.88	.46
62	2.68	.11
63	2.53	.36
64	2.22	-.02
65	1.36	-.11
66	1.41	-.09
67	1.65	.26
68	1.44	.15
69	1.12	0
70	-.03	.22
71	-.06	1.11
72	.29	-.31
73	-.09	.58
74	.92	.26
75	1.01	.51
76	.71	.64
77	0	- .46
78	0	.46
79	0	25.58

TABLE 5.4

Lower Limit of Data

Flight	Frequency	Standard Error (dB/sec)	First Significant Data Time from Launch (sec)	Altitude (km)
14.511	2.225	.07	51	61
	3.385	.29	58	74
14.513	2.225	.16	54	65
	5.04	.33	72	91
14.514	2.225	.09	73	65
	5.04	.26	73	92

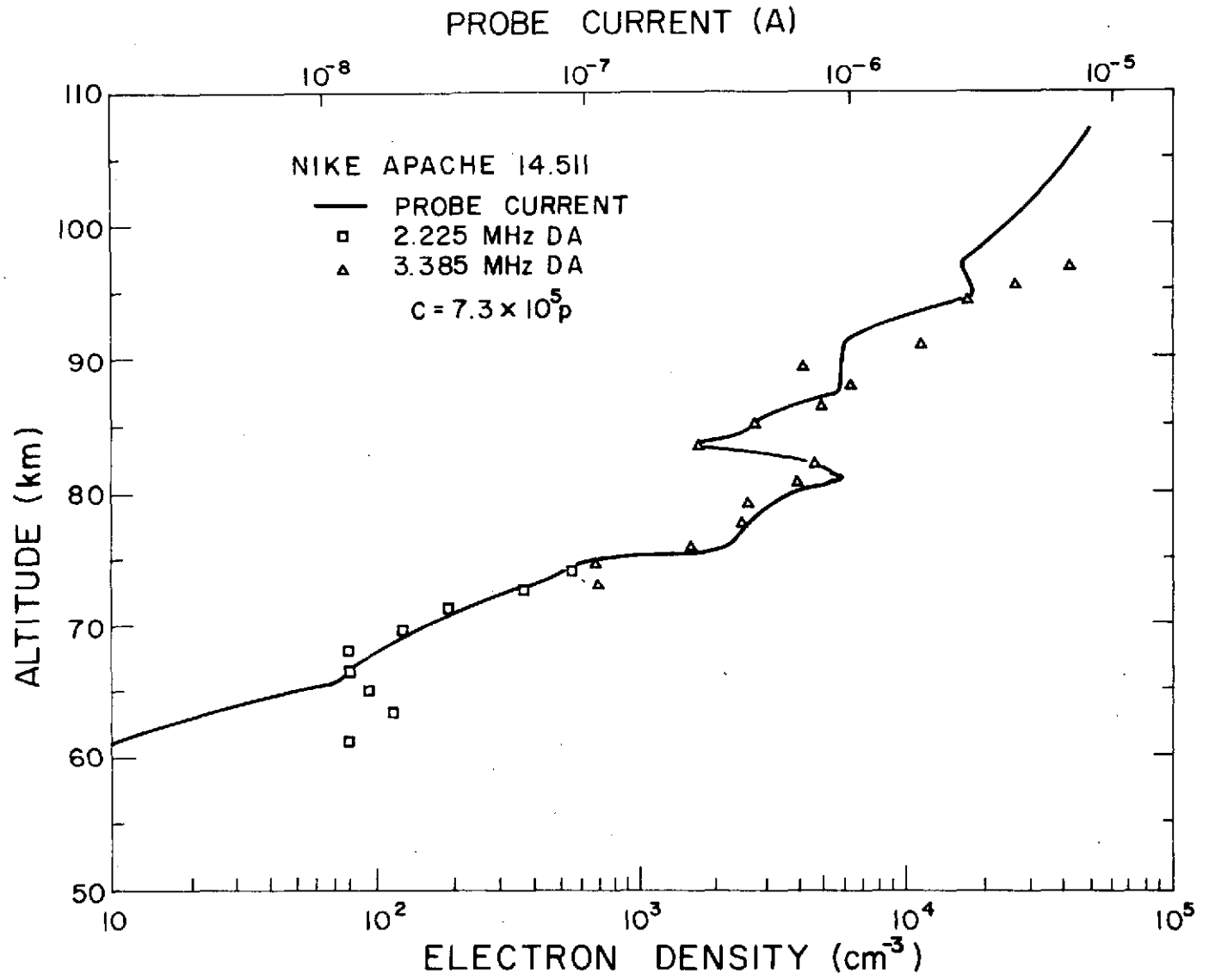

Figure 5.1 Profiles of probe current (upper scale) and electron density (lower scale).

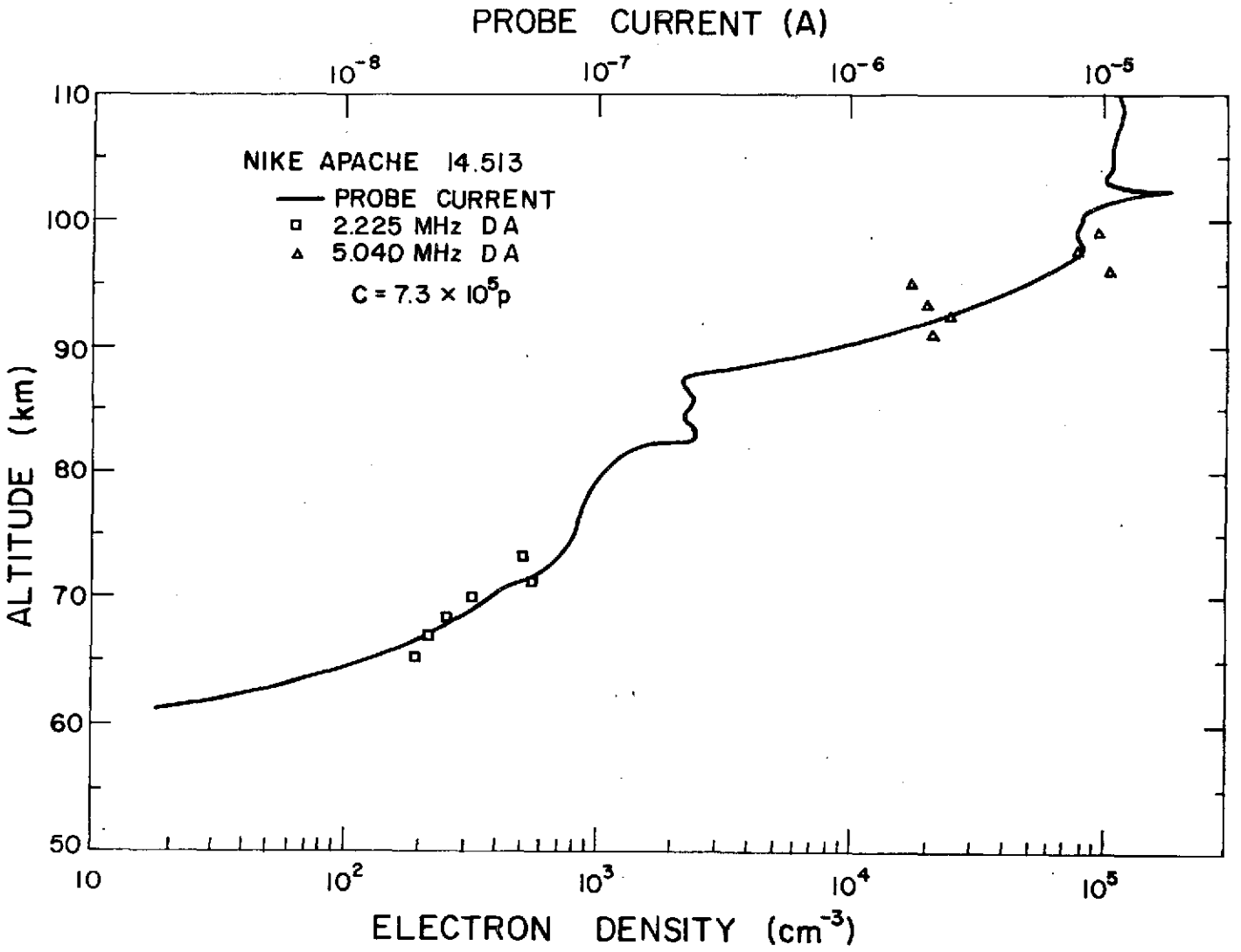

Figure 5.2 Profiles of probe current (upper scale) and electron density (lower scale).

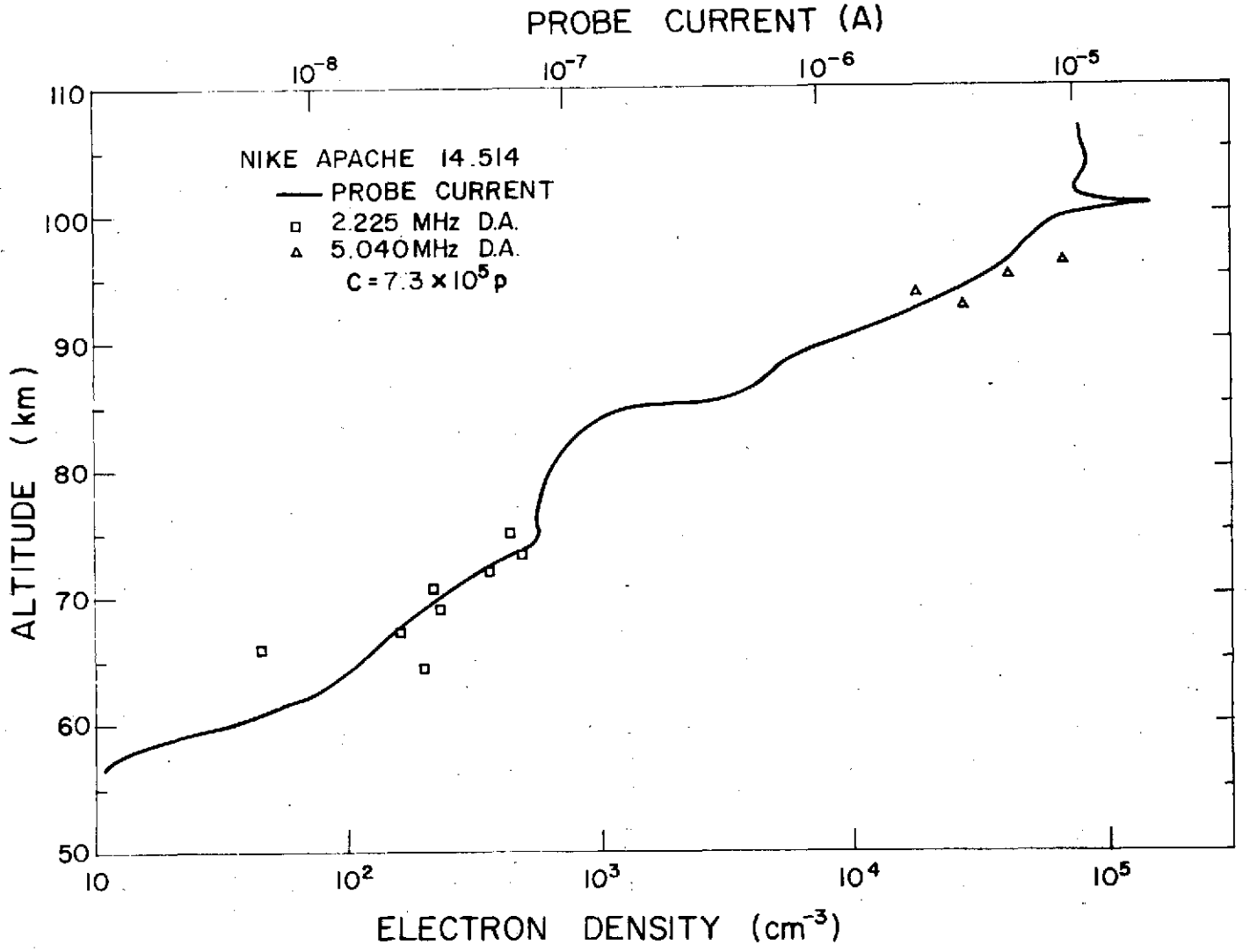

Figure 5.3 Profiles of probe current (upper scale) and electron density (lower scale).

5.2 *Error in Calculated Electron Densities*

The shaded area in Figure 5.4 shows the range over which the electron densities for 14.511 can fall if the errors of up to the standard error in Table 5.1 in the 2225 KHz system are allowed. As would be expected, as the rocket goes further and the rate of absorption increases, the random error represents a smaller portion of the total data. It will be shown below that standard errors previously calculated are not valid above the first few data points, but are a reasonable estimate. Figure 5.5 shows the standard error of each second of data as calculated from the rates of absorption taken one tenth of a second at a time. The magnitude of the error is not in agreement with that calculated in the last section. The reason for this is that the errors are not independent because of the feedback in the system. If the servo moves too fast, resulting in a high absorption rate being recorded, the feedback will result in some data where the rate is slower as the servo returns to its proper setting. The result is that the time over which data are averaged affects the statistics in that the longer the time the more closely the errors approximate independent random values. For this reason, the error values in Figure 5.5 are of larger magnitude than when whole seconds of data were taken at a time. To limit the effect of real absorption, the errors are calculated from a straight line fit of the data generated for that second. Clearly the result shows that as the rocket penetrates the ionosphere the errors increase. The error is increasing at a rate near a factor of two for every ten kilometers of ionosphere traveled through. If this factor is used starting from the first valid point, the error range shown by the dotted line in Figure 5.4 results.

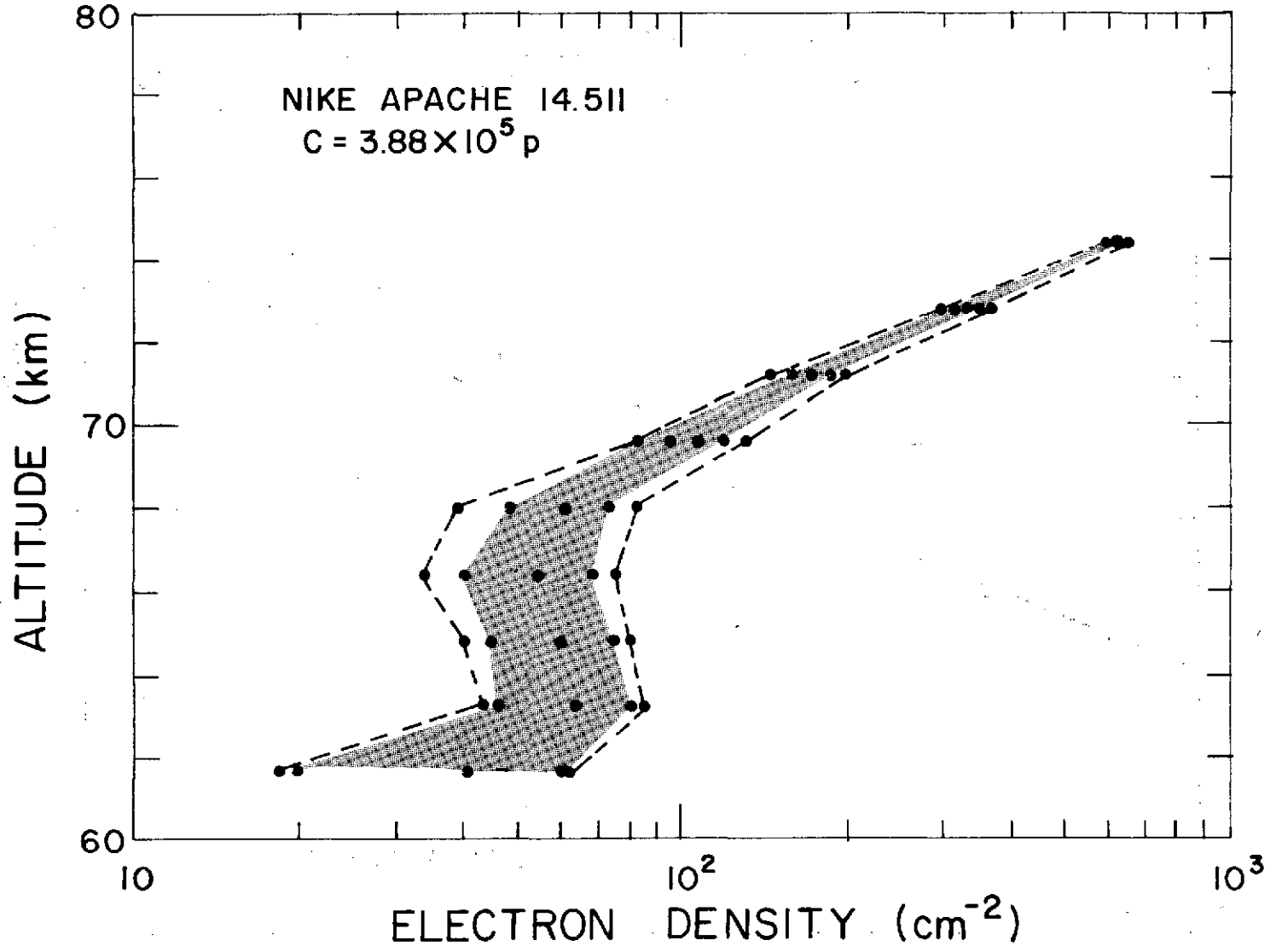

Figure 5.4 Estimated error in electron density.

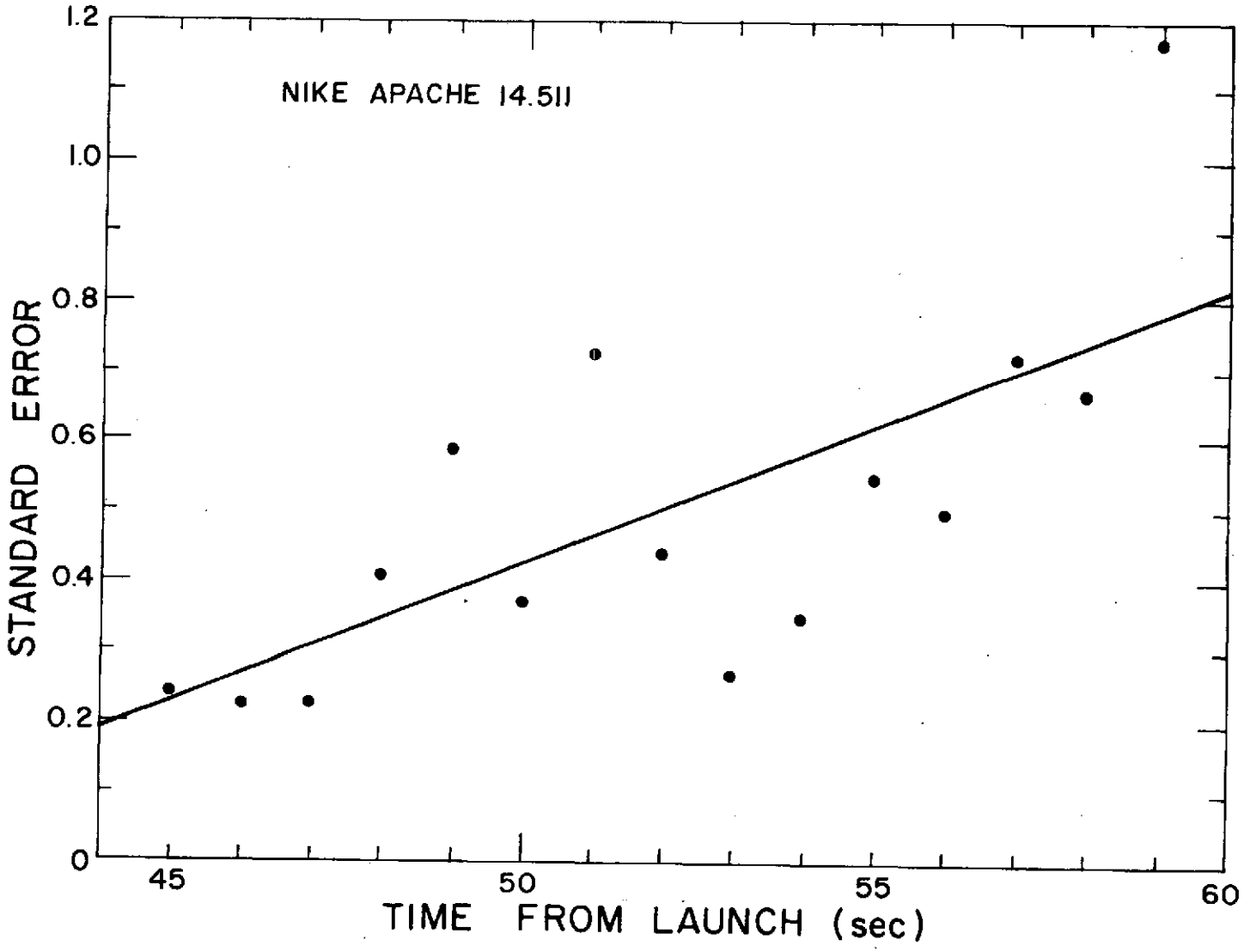

Figure 5.5 Standard error of 1/10 sec data taken over one second.

5.3 *Collision Frequency*

Mechtly [1974] discussed the problem of analyzing differential absorption data in the absence of Faraday rotation. It will be recalled that under these conditions a collision frequency model of the form $\nu_m = C \times 10^5 p$ is used. Figure 5.6 shows the results of using $C = 3.88$ and $C = 7.3$ on the data from 14.511. Looking at Figure 2.1 one notices that using the Sen-Wyller formulation, the absorption is nearly independent of collision frequency at 72 km. This is confirmed by the crossing of the two curves in Figure 5.6 near this altitude.

At points where the data starts, near 62 km, the error between the curves resulting from the choice of C, is greater than that due to inaccuracy in the measurement of the absorption rates. One point that should be noted is that at the 72 km point both errors in measurement and of collision frequency selection are only a small fraction of the total electron concentration. This means that if the probe experiments electron concentration to current ratio is constant in the lower ionosphere the 72 km point becomes an excellent calibration point.

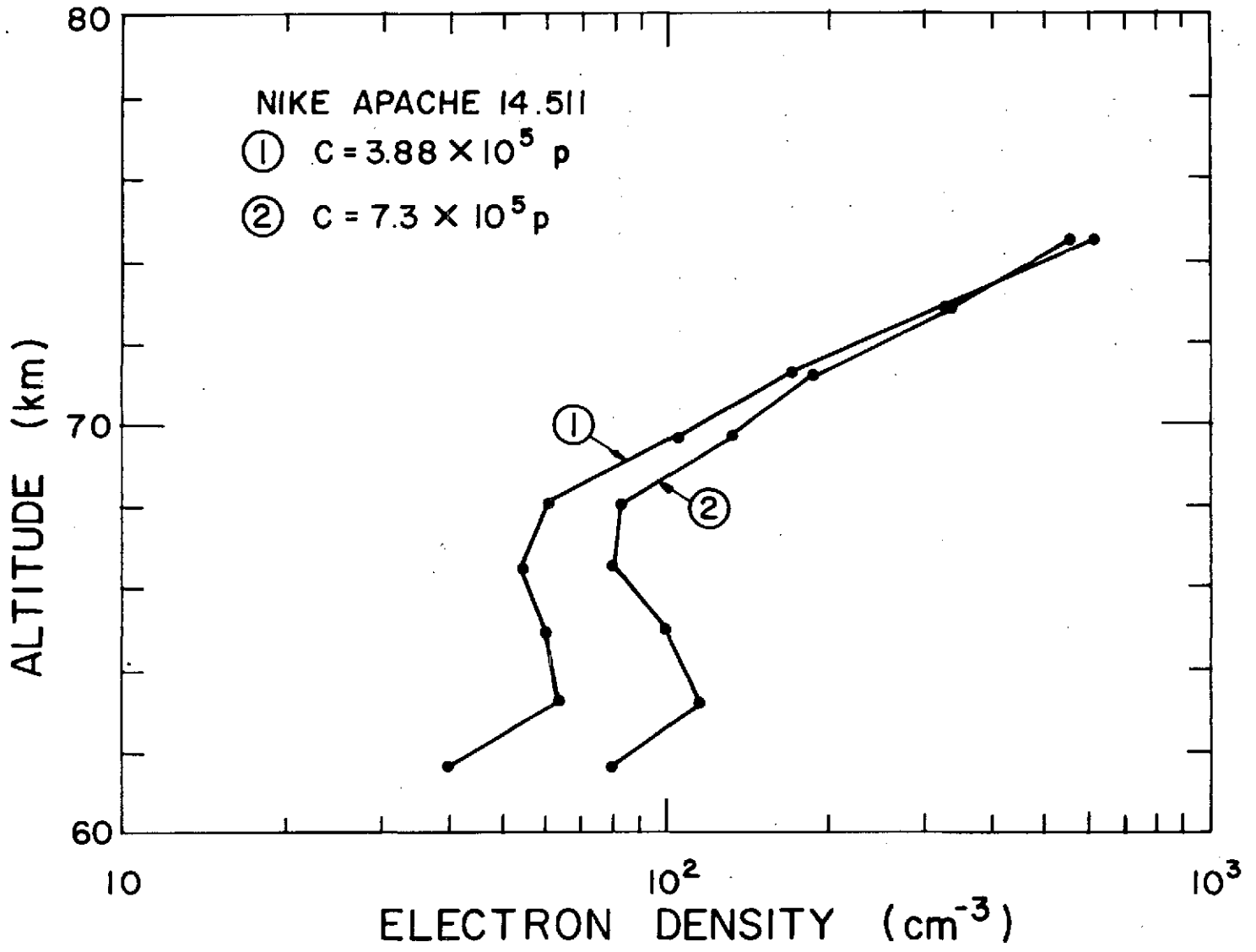

Figure 5.6 Electron densities using different collision frequency models.

6. CONCLUSIONS AND RECOMMENDATIONS

6.1 *Areas of Experiments Usefulness*

As a result of careful examination of experimental equipment and procedures, it is felt that the objective of improving the experiment to a point where electron concentrations on the order of 10 cm^{-3} are measured, is not obtainable, without major system changes. The level to which the experiment can be used is a function of the absorption the wave goes through. 14.511 which was launched on a day of high absorption allowed the experiment to be used down to about 100 cm^{-3}. The other day shots examined, 14.513 and 14.514, for which the absorption was not as high, were useful to levels of 200 cm^{-3}. For nighttime shots with little absorption, the experiment is generally rendered useless by reflections.

As a result of the analysis of where the data can be used, the 2.225 MHz system is found to be useful in the day generally only between 65 and 75 kilometers. The use of the 5.04 MHz system is useful only over an area of about five kilometers. The 3.385 MHz, not generally used in the day, is found to work reasonably well giving much more information than available from the 5.04 MHz system.

6.2 *System Change Recommendations*

The following are suggestions for changes in the system which will lead to improved operation of the differential absorption experiment. None of these changes will degrade the operation of the Faraday rotation experiment.

6.2.1 *Polarization.* To stop the servo system from following the 2δ signal generated by the error signals, filters can be employed. Two

possibilities exist. A notch filter set to eliminate any signal at 2δ can be used, or a bandpass filter centered at $2\delta + 2\omega_r$ with enough attenuation at 2δ to effectively make it 0. For either system, the filter would have to be bypassed for ground tests and during early stages of flight before the spin rate becomes appreciable. The bandpass filter has a disadvantage in that different characteristics would be needed for rockets using different spin rates. The filter must be of very narrow characteristics in a slow spin rocket since it would be desirable to have 40 dB of attenuation in the 2δ signal only $2\omega_r$ radians/sec away from the center of the passband. Some of the bandpass filter's faults could be overcome by the use of a tracking filter which will follow the signal as the spin rate changes. These could be set at 2δ at launch and would then follow the signal as the spin rate builds up, providing constant system lock.

For the notch filter only one need be designed centered at 2δ. It should provide 20 dB of attenuation at 2δ and essentially none at $2\delta + 2\omega_r$ when the smallest spin rate is present in the area of data considered.

In addition to filtering to separate the 2δ and $2\delta + 2\omega_r$ signals, an improved filter to separate the dc component is needed. The servo has been noted to follow the $2\omega_r$ modulation present. The present filter is a first order filter at 1 Hz. It would be desirable to replace this by one with an upper 3 dB point at 2 Hz and with attenuation of 40 dB at about 8 Hz. This dc filter would most likely improve the standard error of the measurements.

It may be advisable to change the value of δ, which is now 250 Hz, if a filter is used. By changing δ down to 50 the Q's of the filter

sections can be reduced by a factor of 5 making stability of the filter less of a problem. This would require, however, redesign of the modulation detector.

Another approach to the problem is to improve the actual polarization characteristics. This is not deemed practical, as an improvement of a factor of about 50 would be needed. This type of improvement could not be obtained with a simple antenna system required for field operation.

6.2.2 *Receivers.* As noted in Chapter 4 the receivers have many undesirable characteristics. These characteristics have been worse in the newer receivers. Since the receivers were originally designed in the early 60's many improvements in techniques have been made. It is suggested that new receivers be designed. These new receivers need not be as sensitive as those presently used. Any sensitivity beyond that necessary to detect the propagating wave, after going through 30 dB of attenuation, will only result in increased noise pickup.

6.3 *Data Reduction*

Most of the improvements in this area are under way. The data now comes digitized on tapes, eliminating that step in the processing. What needs to be done now is to streamline the processing by reducing the amount of human data handling. A start in this area is being made by having each program punch its results onto cards with the appropriate data for the next step. The goal should be to design the processing so that two sets of cards are generated, one with differential absorption data and trajectory, and the other with Faraday rotation data and trajectory. These could then be used in a single program to generate electron densities.

6.4 *Further Test Suggestions*

The effect the telemetry system has on the accuracy of the experiment was not studied. It would be desirable to make a few tests while the rocket is on the ground to measure the accuracy of the telemetry system. One test would be to operate all systems as if under flight conditions and record the servo systems movements. This will test the noise generated by the transmitter to rocket to telemetry station to van loop. Next simulate the expected receiver output at the VCO's in the payload to eliminate the transmitter to rocket section of the loop. Finally, simulate the expected inputs to the data lines at the telemetry station to test the line and the modulation measuring equipment in the van.

If the test of the loop shows errors in recording on the order of .07 dB/sec when analyzed as real data, the loop may be the source of most of the experiment's errors. The further tests will help evaluate where the most improvement can be made.

REFERENCES

Appleton, E. V. (1932), Wireless studies of the ionosphere, *J. Instn. Elec. Engrs.* 71, 642-650.

Edwards, B. (1973), Research in Aeronomy: October 1, 1972-March 31, 1973, *Prog. Rep. 73-1*, Aeron. Lab., Dep. Elec. Eng., Univ. Ill., Urbana-Champaign.

Hartree, D. R. (1931). The propagation of electro-magnetic waves in a refracting medium in a magnetic field, *Proc. Cambridge Phil. Soc. 27*, 143-162.

Jordan, E. C. and K. G. Balmain (1968), *Electromagnetic Waves and Radiating Systems*, Prentice-Hall, Inc., Englewood Cliffs, New Jersey.

Knoebel, H., D. Skaperdas, J. Gooch, B. Kirkwood, and H. Krone (1965), High resolution radio frequency measurements of Faraday rotation and differential absorption with rocket probes, *Coord. Sci. Lab. Rep. R-273*, Univ. Ill., Urbana-Champaign.

Mechtly, E. A., S. A. Bowhill, L. G. Smith, and H. Knoebel (1967), Lower ionosphere electron concentration and collision frequency from rocket measurements of Faraday rotation, differential absorption, and probe current, *J. Geophys. Res. 72*, 5239.

Mechtly, E. A. (1974), Accuracy of rocket measurements of lower ionosphere electron concentrations, *Radio Sci. 9*, 373-378.

Salah, J. E., and S. A. Bowhill (1966), Collision frequencies and electron temperatures in the lower ionosphere, *Aeron. Rep. No. 14*, Aeron. Lab., Dep. Elec. Eng., Univ. Ill., Urbana-Champaign.

Sen, H. K., and A. A. Wyller (1960), On the generalization of the Appleton-Hartree magnetoionic formulas, *J. Geophys. Res. 65*, 3931-3950.

Slekys, A. G., and E. A. Mechtly (1970), Aeronomy Laboratory system for digital processing of rocket telemetry tapes, *Aeron. Rep. No. 35*, Aeron. Lab., Dep. Elec. Eng., Univ. Ill., Urbana-Champaign.

Taub, H., and R. L. Schilling (1971), *Principles of Communication Systems*, McGraw-Hill, Inc., New York, 268-319.